LARGE-SCALE BIOLOGY ARTICLE

A PXY-Mediated Transcriptional Network Integrates Signaling Mechanisms to Control Vascular Development in Arabidopsis

Margot E. Smit[1,2,3]•, Shauni McGregor[4,5]•, Heng Sun[6], Catherine Gough[4], Anne-Maarit Bågman[1], Cara L. Soyars[7,8], Johannes T. Kroon[4], Allison Gaudinier[1,9], Clara J. Williams[1,10], Xiyan Yang[6], Zachary L. Nimchuk[7], Dolf Weijers[2], Simon R. Turner[11], Siobhán M. Brady*[1] and J. Peter Etchells*[1,4]

[1] University of California Davis, Plant Biology & Genome Center, Davis, California, 95616, USA
[2] Laboratory of Biochemistry, Wageningen University, the Netherlands.
[3] Stanford University, Stanford, CA, USA, 94305-5020
[4] Durham University, Department of Biosciences, Durham, DH1 3LE, UK
[5] Current address: University of Sheffield, APS, Western Bank
[6] National Key Laboratory of Crop Genetic Improvement, Huazhong Agricultural University, Wuhan, Hubei, 430070, PR China
[7] Department of Biology, University of North Carolina at Chapel Hill, Chapel Hill, North Carolina, USA.
[8] Thermo Fisher Scientific
[9] Department of Plant and Microbial Biology, University of California Berkeley, CA 94720, USA
[10] Current address: UGhent, VIB Department of Plant Systems Biology, Belgium.
[11] University of Manchester, Faculty of Life Sciences, Manchester, M13 9PT, UK.
• Equal contribution
*Corresponding authors: Peter.Etchells@durham.ac.uk; sbrady@ucdavis.edu

Short title: An Arabidopsis vascular development network

One sentence summary: A feed-forward loop that controls vascular development was uncovered by identifying a transcriptional network mediated by the receptor kinase PHLOEM INTERCALATED WITH XYLEM.

The authors responsible for distribution of materials integral to the findings in this article in accordance with the policy described in the instructions for authors (www.plantcell.org) are J. Peter Etchells (Peter.Etchells@durham.ac.uk) and Siobhán M. Brady (sbrady@ucdavis.edu)

ABSTRACT

The cambium and procambium generate the majority of biomass in vascular plants. These meristems constitute a bifacial stem cell population from which xylem and phloem are specified on opposing sides by positional signals. The PHLOEM INTERCALATED WITH XYLEM (PXY) receptor kinase promotes vascular cell division and organisation. However, how these functions are specified and integrated is unknown. Here, we mapped a putative

PXY-mediated transcriptional regulatory network comprising 690 transcription factor-promoter interactions in *Arabidopsis thaliana* (Arabidopsis). Among these interactions was a feed-forward loop containing transcription factors WUSCHEL HOMEOBOX RELATED14 (WOX14) and TARGET OF MONOPTEROS6 (TMO6), which each regulate the expression of the gene encoding a third transcription factor, LATERAL ORGAN BOUNDARIES DOMAIN4 (LBD4). PXY signalling in turn regulates the WOX14, TMO6, LBD4 loop to control vascular proliferation. Genetic interaction between *LBD4* and *PXY* suggests that LBD4 marks the phloem-procambium boundary, thus defining the shape of the vascular bundle. These data collectively support a mechanism that influences recruitment of cells into the phloem lineage, and they define the role of PXY signalling in this context in determining the arrangement of vascular tissue.

INTRODUCTION

In vascular plants, water is taken up from the soil but sugars are assimilated in leaves, so the movement of these resources throughout the plant body is essential for plant survival. Xylem and phloem are the specialized vascular tissues that perform this function. Both arise in a highly ordered manner from meristematic divisions in the cambium and procambium. Multiple mechanisms have been identified that influence vascular development (Fischer et al., 2019); however, how these mechanisms interact to coordinate vascular morphogenesis is poorly understood.

Auxin is central to vascular tissue specification, and its responses are mediated by, among others, *MONOPTEROS* (*MP*), which encodes an Auxin Response Factor (ARF) (Hardtke and Berleth, 1998). *Arabidopsis thaliana* (Arabidopsis) *mp* mutants are characterised by patterning defects in the embryo vascular cylinder (Berleth and Jurgens, 1993). *MP* is thought to act as an activator of vascular proliferation in seedlings (Vera-Sirera et al., 2015) or as a repressor of vascular proliferation in mature plant tissues (Mattsson et al., 2003; Brackmann et al., 2018). With additional signals, MP controls two pathways that stimulate vascular proliferation. The first pathway is characterised by *TARGET OF MONOPTEROS5* (*TMO5*), encoding a bHLH transcription factor (Schlereth et al., 2010) that with its homologues promotes cell divisions in the vascular cylinder. These transcription factor genes are up-regulated by MP in the embryo. TMO5-like proteins perform this function in heterodimers with a second class of bHLH transcription factors including LONESOME HIGHWAY and its relatives (Ohashi-Ito and Bergmann, 2007; De Rybel et al., 2013; De Rybel et al., 2014; Ohashi-Ito et al., 2014; Vera-Sirera et al., 2015). The second pathway targeted by MP comprises the auxin-responsive *TMO6* (Schlereth et al., 2010), which encodes a member of

the DOF family of transcription factors. Multiple members of the DOF family have been shown to promote vascular cell divisions (Guo et al., 2009; Waki et al., 2013; Konishi et al., 2015; Miyashima et al., 2019; Smet et al., 2019). The expression of a subset of *DOF* genes, including *TMO6*, is also controlled by cytokinin (Miyashima et al., 2019). Thus, *TMO6* responds to both cytokinin and auxin.

TRACHEARY ELEMENT DIFFERENTIATION INHIBITORY FACTOR (TDIF) and PHLOEM INTERCALATED WITH XYLEM/TDIF RECEPTOR (PXY/TDR; referred to hereafter as PXY) are a ligand-receptor pair (Hirakawa et al., 2008; Morita et al., 2016; Zhang et al., 2016) that also promotes cell division in vascular meristems. The TDIF peptide is derived from *CLE41*, *CLE42* and *CLE44*. These genes are expressed in the phloem while *PXY* is expressed in the procambium (Ito et al., 2006; Fisher and Turner, 2007; Hirakawa et al., 2008; Etchells and Turner, 2010). Upon TDIF binding to the PXY receptor, the transcription factor genes *WOX4*, *WOX14*, and *ATHB8* are upregulated (Hirakawa et al., 2010; Etchells et al., 2013). Another transcription factor, BES1, is also regulated by TDIF-PXY. When TDIF binds to PXY, an interaction between PXY and GSK3 kinases results in the phosphorylation and degradation of BES1. BES1 is thought to promote xylem differentiation, so its degradation preserves cambium pluripotency (Kondo et al., 2014).

Interactions between TDIF-PXY and auxin signalling contribute to vascular tissue development (Suer et al., 2011; Smetana et al., 2019). Both auxin and PXY responses are mediated by interactions with GSK3 signalling proteins. GSK3s regulate the auxin response via phosphorylation of ARFs, and during vascular development, this requires the absence of active TDIF-PXY complexes (Cho et al., 2014; Kondo et al., 2014; Han et al., 2018). Auxin also induces the expression of TDIF-PXY targets *ATHB8* and *WOX4* (Baima et al., 1995; Mattsson et al., 2003; Suer et al., 2011). The induction of *TMO5-like1* (*T5L1*) and *LHW* also increases *ATHB8* expression (Vera-Sirera et al., 2015). *ATHB8* encodes a HD-Zip III transcription factor (Baima et al., 2001) whose paralogues modulate the expression of auxin biosynthesis and auxin perception genes (Müller et al., 2016). HD-Zip III genes have wide-ranging roles in vascular patterning and proliferation (Zhong and Ye, 1999; Emery et al., 2003; Prigge et al., 2005; Carlsbecker et al., 2010; Baima et al., 2014; Ramachandran et al., 2016).

In addition to PXY, a second family of receptor kinases, members of the ERECTA (ER) family, control vascular expansion in Arabidopsis (Ragni et al., 2011; Uchida et al., 2012; Uchida and Tasaka, 2013; Ikematsu et al., 2017). *PXY* and its paralogues genetically interact with *ER* family members to control proliferation, cell size, and organisation in vascular tissues (Etchells et al., 2013; Uchida and Tasaka, 2013; Wang et al., 2019). *ER* also interacts with auxin signalling components and members of the HD-ZipIII family in developmental contexts that include meristem maintenance, stem architecture, and leaf development (Woodward et al., 2005; Chen et al., 2013). Thus, interactions between *PXY*, auxin, cytokinin, *HD-Zip III*s, *ER*, and GSK3s constitute a significant proportion of the regulatory mechanisms that define how vascular tissue develops.

How do these and other factors combine to coordinate vascular development at the level of transcription? Here, to provide a framework for answering this question, we generated a transcriptional regulatory network (TRN) incorporating a significant proportion of known regulators of vascular development in Arabidopsis. We used high-throughput enhanced yeast-one-hybrid (eY1H) assays (Gaudinier et al., 2011; Reece-Hoyes et al., 2011; Gaudinier et al., 2017) to identify transcription factors that bind to the promoters of vascular regulators. Our vascular development TRN comprises 690 transcription factor-promoter interactions. To demonstrate the power of our network to identify novel regulators and interactions, we characterised a feed-forward loop incorporating three transcription factors that link auxin and PXY-mediated signalling: WOX14, TMO6, and LATERAL ORGAN BOUNDARIES DOMAIN4 (LBD4). Feed-forward loops are often involved in dynamic gene regulation (Mangan and Alon, 2003), and our results demonstrate that, in response to auxin and TDIF-PXY signalling, the genes within this circuit define a zone of procambial activity to maintain the arrangement of vascular tissue of the stem.

RESULTS

Identification of putative TDIF target genes

To generate a TRN downstream of TDIF, we first identified putative TDIF target genes. The TDIF peptide ligand is derived from CLE41, CLE42 and CLE44 proteins, so we compared the transcriptomes of mature (5-week-old) stem bases of *35S:CLE41* lines (i.e. increased PXY signalling), to wild type. Genes were considered differentially expressed where the p-value, adjusted for multiple hypothesis testing, was ≤0.05 (**Supplemental Data Set 1**). *35S:CLE41* plants had on average 100.7 ± 9.1 undifferentiated cells per vascular bundle

compared to 59.5 ± 5.5 in the wild type (**Supplemental Figure 1A, B**). Consistent with the vascular over-proliferation phenotype, genes shown to be predominantly expressed in the procambium, including *BRI-LIKE1*, *PINFORMED1*, and *MP* (Gälweiler et al., 1998; Hardtke and Berleth, 1998; Cano-Delgado et al., 2004), demonstrated significant increases in expression in *35S:CLE41* plants relative to wild type (**Supplemental Table 1**). The expression levels of previously described targets of PXY signalling, *ATHB8* and *WOX14* (Hirakawa et al., 2010; Etchells et al., 2013), increased 2.78-fold (p<0.001) and 4.76-fold, respectively, in *35S:CLE41* vs. the wild type (p<0.001). Our microarray data were further validated using qRT-PCR of a select number of genes involved in xylem cell differentiation or transcriptional regulation, including an *ASPARTIC PEPTIDASE* gene, *GMC OXIDOREDUCTASE, MAP70-5*, *IAA30*, and *MYB38* (**Supplemental Figure 1**), and were consequently used to guide promoter selection for eY1H experiments.

A PXY-mediated transcriptional network for vascular development

To understand how factors that control PXY-mediated vascular development interact, and to identify novel vascular regulators, we identified transcription factor-promoter interactions using enhanced Y1H assays (Gaudinier et al., 2011; Reece-Hoyes et al., 2011). Bait were selected promoters from five groups of genes representing factors that regulate PXY-mediated or xylem cell development in the inflorescence stem (**Supplemental Table 2**). Group I included *PXY* and *PXL* receptors (Fisher and Turner, 2007), ligands (Ito et al., 2006), and their target transcription factor gene, *WOX14* (Etchells et al., 2013). Group II comprised *GSK3* family members, which interact with the PXY kinase domain (Kondo et al., 2014), and their target transcription factor genes *BES1* and *BZR1* (He et al., 2002). The *ERECTA* family (*ER*f) of receptors were included in group II, as ER-family receptors act in part through GSK3 signalling (Kim et al., 2012), and they genetically interact with PXY-family receptors (Wang et al., 2019). Genes involved in auxin or cytokinin perception and auxin responses that also demonstrated differential expression in *35S:CLE41* constituted groups III and IV. These included *TMO6*, a transcriptional target of MP (Schlereth et al., 2010) and its paralog *DOF1.8* (Le Hir and Bellini, 2013) (**Supplemental Table 2**). Promoters of *HD Zip-III* transcription factor genes that were differentially expressed in *35S:CLE41* lines and have been shown elsewhere to control vascular development (Zhong and Ye, 1999; Baima et al., 2001; McConnell et al., 2001; Emery et al., 2003; Carlsbecker et al., 2010; Müller et al., 2016) were used as bait for group V. Finally, based on very high expression in *35S:CLE41*,

LBD4/ASL6 and its homologue, *LBD3*/*ASL9*, genes of unknown function were identified (**Supplemental Table 2**).

We screened these promoters against a collection of 812 root-expressed transcription factors that represent more than 95% of the transcription factors with enriched expression in the Arabidopsis stele (Gaudinier et al., 2011; Taylor-Teeples et al., 2015). The resulting interactions comprise a network consisting of 312 nodes (**Figure 1A**). Each node represents a gene either as a promoter, as a transcription factor, or as both. The nodes were connected by 690 edges, each representing a transcription factor binding to a promoter, as identified in the eY1H assays (**Figure 1A, Supplemental Data Set 2**). To visualize the nodes and edges, we designed a custom layout in Cytoscape (Shannon et al., 2003). Promoter nodes were colored and arranged in the five association groups described in the previous paragraph, i.e., PXY signaling (group I; blue), ER/BRI1/GSK3 signaling (group II; mint), auxin/cytokinin perception (group III green/red), targets of MP and affiliates (group IV orange/purple), and HD-ZIPIIIs (group V, olive) (**Figure 1A**). Transcription factors are colored in white and positioned in the network based on their target profile. Those targeting similar sets of genes/groups were placed together. Transcription factors interacting with promoters in more than two groups were placed at the center of the network. Those interacting with one or two promoter groups were placed on the periphery. In total, 287 transcription factors targeted at least one promoter in the network. The transcription factor families with the greatest representation were AP2/EREBP transcription factors, of which 46 members interacted with the screened promoters, followed by MYB (40 interactors), and C2H2 transcription factors (31 interactors). A list of all interacting transcription factors and their respective classes is shown in **Supplemental Data Set 3**).

We predicted that the network would be enriched for genes differentially expressed in *35S:CLE41* (**Supplemental Figure 2A**). A significant enrichment ($p = 2.2e-6$) was observed using a Fisher's exact test. Furthermore, using previously described loss-of-function gene expression data from *pxy* mutants (Etchells et al., 2012), a more dramatic enrichment ($p = 1.57e-62$; **Supplemental Figure 2B**) was observed. Thus, the network represents a PXY-mediated transcriptional regulatory network.

A WOX14-mediated feed-forward loop

We used our predicted vascular development network (**Figure 1A**) combined with our *35S:CLE41* transcriptome data (**Supplemental Data Set 1**) to identify a regulatory circuit for further analysis. Promoters were ranked by the number of transcription factors that bound to them (in-degree binding). *PHB*, *PHV*, *LBD4*, and *T5L1* demonstrated the highest levels of in-degree connectivity in our TRN (**Supplemental Data Set 4**). In addition to its high in-degree value of 68 (ranked 3rd), *LBD4* also demonstrated an 11-fold increase in expression in *35S:CLE41* vs. the wild type (**Supplemental Table 1; Supplemental Data Set 1**), higher than that of any other transcription factor. Furthermore, its function had not previously been described, making it a strong candidate for further investigation.

TMO6 and WOX14 were predicted to bind to and regulate *LBD4* (**Figure 1B**; **Supplemental Data Set 2**). Both were also expressed to a high degree in *35S:CLE41* lines, each demonstrating a 4.8-fold increase in expression (**Supplemental Table 2, Supplemental Data Set 1**). WOX14 was also predicted to bind to and regulate both *TMO6* and *LBD4* (**Figure 1B**; **Supplemental Data Set 2**); thus, these three transcription factors were present in a feed-forward loop (**Figure 1B**). Feed-forward loops are enriched within xylem regulatory networks (Taylor-Teeples et al., 2015) and ensure robust regulation of their target genes (Shen-Orr et al., 2002; Mangan and Alon, 2003; Kalir et al., 2005; Kaplan et al., 2008). We hypothesized that the WOX14-TMO6-LBD4 feed-forward loop plays a key role in regulating vascular development due to its potential to integrate auxin, cytokinin, and TDIF-PXY signalling (**Figure 1A-B**). Specifically, *TMO6* is transcriptionally regulated by both auxin (Schlereth et al., 2010) and cytokinin (Miyashima et al., 2019; Smet et al., 2019). *WOX14* is regulated by TDIF-PXY (Etchells et al., 2013). Consequently, based on high network connectivity and high expression in *35S:CLE41* relative to wild type, their likelihood of integrating PXY, auxin, and cytokinin signalling, and their arrangement in a feed-forward loop, we selected the regulatory circuit involving TMO6, WOX14, and LBD4 for further study.

Genetic elimination of the *TMO6-WOX14-LBD4* feed-forward loop

To determine the significance of the *TMO6-WOX14-LBD4* feed-forward loop in vascular development, we genetically perturbed each of these genes singly and in combination. We combined *wox14* (Etchells et al., 2013) and *lbd4* Arabidopsis T-DNA lines with *tmo6* mutants generated by genome editing. The single mutants demonstrated no changes in the number of cells per vascular bundle or vascular morphology compared to the wild type

(**Figure 2A, F-G**; **Figure 3G**, **J-K**; **Supplemental Figure 3A-B, E-G**; Etchells et al., 2013). By contrast, the number of cells present per vascular bundle was significantly reduced in *tmo6 wox14 lbd4* triple and *tmo6 wox14* double mutant stems ($p < 0.002$ and $p = 0.002$; **Figure 2A-F; Supplemental Data Set 5**). Consistent with TMO6 and WOX14 acting as upstream regulators of *LBD4*, as predicted from the eY1H data (**Figure 1A**), the *tmo6 wox14* and *tmo6 wox14 lbd4* lines were indistinguishable ($p = 0.371$; **Figure 2D, F**).

In the wild type, vascular bundles expand to a greater degree along the radial axis of the stem than the tangential, and thus vascular bundle shape can be measured by comparing tangential:radial ratios. In the *tmo6 wox14 lbd4* lines, this ratio was higher than in wild type (**Figure 2G**), and as such, the triple mutant demonstrated reduced expansion along the radial axis of the stem. This genetic interaction supports the idea that the feed-forward loop transcription factors are components of the same pathway and that they are critical for controlling vascular proliferation and shape.

WOX14 and TMO6 are sufficient to regulate gene expression within the feed-forward loop in plant cells

A prerequisite for *in planta* transcriptional regulation within the feed-forward loop is the expression of *TMO6*, *WOX14*, and *LBD4* in the same place and time. Using *in situ* hybridization, *TMO6* and *LBD4* mRNA antisense probes hybridised to cells in the vascular tissue of the inflorescence stem, with expression maxima at the phloem-procambium boundary (**Figure 3A-B, Supplemental Figure 4A** for sense controls). *WOX14:GUS* expression (**Figure 3C**) was also present in phloem-procambium boundary cells, in addition to other vascular cell types, and as described previously (Etchells et al., 2013).

Given the genetic interaction and overlapping expression of *TMO6*, *WOX14*, and *LBD4*, we sought more direct evidence for the feed-forward loop interactions identified in eY1H *in planta*. We transformed wild tobacco (*Nicotiana benthamiana*) leaf protoplasts with a construct that harboured *LBD4pro:LUC* (*LUCIFERASE*) and *35S:REN* (*RENILLA*) cassettes and determined *LBD4pro* activity as LUC activity normalised to that of REN. LUC activity was higher in cells co-transformed with both *LBD4pro:LUC* reporter and a *35S:TMO6* construct than in cells transformed with the *LBD4pro:LUC* reporter and a control (empty vector) construct ($p<0.001$; **Supplemental Figure 5A**). *LBD4* promoter activity further increased ($p=0.005$) when cells were co-transformed with *LBD4pro:LUC*, *35S:TMO6*, and

35S:WOX14. The LUC activity in cells containing both *LBD4pro:LUC* and *35S:WOX14* was similar to that in cells harbouring *LBD4pro:LUC* and an empty vector control.

We used a similar strategy to verify WOX14-mediated regulation of transcripts under the control of the *TMO6* promoter. Here, LUC activity was significantly higher ($p<0.001$) when *TMO6pro:LUC* was co-transformed with a *35S:WOX14* construct than when transformed with a control construct (**Supplemental Figure 5B**). In summary, these multiple pieces of data provide evidence that the WOX14-TMO6-LBD4 transcription factor-promoter interactions are sufficient to regulate transcription in plant cells (**Supplemental Figure 5**).

Interconnected transcriptional regulation in the feed-forward loop

We obtained *in planta* genetic evidence for these regulatory relationships by performing qRT-PCR and examining loss-of-function mutant alleles. Our network suggested that *LBD4* and *TMO6* act downstream of *WOX14* (**Figure 1B**), so we tested the expression levels of these genes in *wox14* mutants in the basal third of 15 cm inflorescence stems, where *WOX14* expression had previously been shown to be the highest. Because *WOX14* acts redundantly with *WOX4* (Etchells et al., 2013), *wox4* and *wox4 wox14* lines were also included in our analysis. Consistent with the notion that WOX14 regulates *TMO6* and *LBD4* expression, *wox14* stems exhibited lower levels of *TMO6* and *LBD4* expression than wild type (**Figure 3D-E**). Thus, wild-type levels of *TMO6* and *LBD4* expression are dependent on the expression of *WOX14*. Further reductions in *TMO6* and *LBD4* expression were not observed in *wox4 wox14* lines relative to single *wox4* or *wox14* mutant alleles.

To determine if *LBD4* expression is also dependent on *TMO6* expression (**Figure 1B**), we tested *tmo6* mutant lines. In the basal half of 15 cm inflorescence stems, *LBD4* expression was unchanged in *tmo6* relative to wild type (**Figure 3F; Supplemental Table 3**). We reasoned that the dependency of *LBD4* on *TMO6* might be revealed in a sensitised genetic background. To test this hypothesis, we generated *wox4 wox14 tmo6* and *pxy pxl1 pxl2 tmo6* (*px*f *tmo6*) lines. *tmo6* dramatically enhanced the cell division defect observed in the *px*f triple mutants (**Figure 3G-J; Supplemental Data Set 5**), although the shapes of the bundles (based on the tangential:radial ratio) did not differ from those of the *px*f lines (**Figure 3K**). We measured *LBD4* expression in the lower halves of inflorescence stems. The reductions in *LBD4* expression in both the *px*f and *wox4 wox14* lines proved not to be significant ($p=0.167$ and $p=0.102$; **Figure 3F; Supplemental Table 3**). By contrast, *LBD4* expression was

significantly lower in the *px*f *tmo6* and *wox4 wox14 tmo6* mutants relative to wild type (p=0.031 and p=0.027). Thus, while *LBD4* expression did not depend on the presence of *TMO6* in the lower halves of 15 cm inflorescence stems, the reduced expression was exacerbated in *tmo6 px*f and *tmo6 wox4 wox14* relative to the parental lines (**Figure 3F**). Therefore, *TMO6*, redundantly with TDIF/PXY signalling, regulates *LBD4* expression.

While these results supported the idea that TMO6 and WOX14 regulate *LBD4* expression, they also raised the question of why *LBD4* expression was reduced in *wox4 wox14* lines when the lower third of 15 cm inflorescence stems were sampled (**Figure 3E**), but not when the lower half was sampled (**Figure 3F**). We reasoned that *LBD4* expression may vary along the apical-basal axis of the stem and tested this hypothesis using qRT-PCR. *LBD4* expression was significantly higher in the basal third of the inflorescence stem relative to the middle or apical sections (**Supplemental Figure 4B**), which is consistent with the *LBD4* expression levels observed in **Figures 3E and 3F**.

TDIF-PXY dynamically regulates the feed-forward loop

As *LBD4* expression was reduced in the *px*f *tmo6* background, and *tmo6* genetically enhanced the *px*f phenotype (**Figure 3I-K**), we further explored the expression of genes in this feed-forward loop in response to perturbations in TDIF-PXY signalling. We measured *LBD4* and *TMO6* expression in *px*f (Fisher and Turner, 2007; Wang et al., 2019) and in *cle41 cle42 cle43 cle44* mutants (referred to hereafter as *tdif*; **Supplemental Figure 6**), which were generated by genome editing. Here, specifically, we measured gene expression in the lower third of 10 cm stems. A significant reduction in *LBD4* expression was not observed, but reduced *TMO6* expression was observed (**Figure 4A,B**). These results demonstrate that *TMO6* is responsive to genetic perturbation of TDIF-PXY signalling.

To determine the temporal dynamics of gene regulation within the feed-forward loop, we applied TDIF or control peptide to five-day-old wild type, *pxy*, and *wox4 wox14* seedlings. *WOX14* expression increases upon TDIF application (Etchells et al., 2013). Similarly, a 2-hour treatment with 5 µM TDIF in wild-type plants resulted in increased *LBD4* and *TMO6* expression relative to plants treated with a P9A negative control (**Figure 4C,D**). This induction of *TMO6* and *LBD4* was absent, and their expression even further reduced, in *pxy* and *wox4 wox14* mutants, suggesting that PXY/TDIF activate the expression of all genes within the feed-forward loop (**Figure 4A-D**).

The WOX14-TMO6-LBD4 feed-forward loop is auxin responsive

MP is a transcriptional regulator of *TMO6* (Schlereth et al., 2010), and crosstalk between auxin and TDIF-PXY signalling has been described (Suer et al., 2011; Han et al., 2018). We therefore tested the expression of all three transcription factors in the feed-forward loop upon exposure to 10 μM IAA. *TMO6* and *LBD4* expression increased in response to a 6-hour auxin treatment in both wild type and *wox14* mutants, demonstrating that auxin regulates *LBD4* and *TMO6* expression in a *WOX14*-independent manner (**Figure 4E-F**). *WOX14* was also upregulated in response to auxin treatment (**Figure 4G**).

***LBD4* regulates vascular cell number and organization**

To determine the function of this feed-forward loop in vascular development, we characterized vascular development in inflorescence stems upon genetic perturbation of the final gene within the feed-forward loop, *LBD4*. The phenotype of the *lbd4* single mutant was similar to that of the wild-type controls (**Figure 2F-G; Supplemental Figure 3A-B; Supplemental Data Set 5**). To eliminate functional redundancy, we crossed *lbd4* to a T-DNA insertion line of *LBD3,* the gene most similar to *LBD4* (Shuai et al., 2002). A reduction in vascular cell number was observed in *lbd3 lbd4* double mutants (**Supplemental Figure 3D-E**).

LBD4 is expressed at the procambium-phloem boundary (**Figure 3A**). Thus, we determined phloem cell number in the *lbd3 lbd4* double mutants and controls, but no differences were observed (**Supplemental Figure 3E**; **Supplemental Data Set 5**). We also measured the distribution of phloem along the radial axis in these lines. The *lbd3 lbd4* double mutants had a thinner band of phloem in vascular bundles than the control lines (**Supplemental Figure 3F**), although this did not influence overall vascular bundle shape, as judged by measuring the tangential:radial ratio (**Supplemental Figure 3G**). Other members of the *LBD* gene family define boundaries at the edges of the apical meristem and the lateral root (Okushima et al., 2007; Bell et al., 2012). *LBD4* is expressed at the phloem-procambium boundary and influences phloem distribution redundantly with *LBD3*. Thus, we reasoned that *LBD4* might influence boundaries within vascular tissue. To explore this idea, we manipulated the *LBD4* expression domain. *LBD4* expression was restored ectopically in companion cells of the phloem using a *SUC2:LBD4* construct or in the xylem using an *IRX3:LBD4* construct, both within the *lbd4* mutant background (**Figure 5**). In *lbd4 SUC2:LBD4* lines, an increase in the

382 total number of cells per vascular bundle was observed. While xylem cell number did not
383 differ between genotypes, both phloem and procambium cell numbers were higher in *lbd4*
384 *SUC2:LBD4* than in the other lines (**Figure 5D**).
385
386 We observed reduced secondary cell wall deposition in the fiber cells of *lbd4 IRX3:LBD4*
387 lines (**Figure 5A,C**), indicating that xylem differentiation was disrupted, although the total
388 number of cells in the xylem did not change (**Figure 5D**). In terms of overall vascular bundle
389 shape within these different backgrounds, the ratio of the length of the tangential to radial
390 axes of vascular bundles was 0.65 in wild type, which is similar to that observed in *lbd4* and
391 *lbd4 SUC2:LBD4* lines (**Figure 5E**). By contrast, the ratio increased to 0.96 in *lbd4*
392 *IRX3:LBD4* vascular bundles, demonstrating a reduction in vascular expansion along the
393 radial axis relative to the tangential axis. Furthermore, phloem distribution was dramatically
394 different in the *LBD4* misexpression lines. The *lbd4 SUC2:LBD4* lines exhibited a wider
395 band of phloem along the radial axis compared to the other lines tested (**Figure 5E**). While
396 this can be explained in part by changes to phloem cell number, the same cannot be said of
397 changes to phloem distribution in *lbd4 IRX3:LBD4* lines. Here, despite similar numbers of
398 phloem cells relative to wild type or *lbd4* single mutants (**Figure 5D**), these phloem cells
399 were distributed in a much narrower band (**Figure 5E**). The redistribution of phloem cells
400 accompanied by changes to vascular bundle shape could be caused by a failure to correctly
401 mark the phloem-procambium boundary.
402
403 **The vascular function of LBD4 is PXY/TDIF-dependent**
404 *pxy* and *tdif* mutants demonstrate intercalation of vascular cell types, i.e., a loss of clearly
405 defined boundaries (**Figure 6, Supplemental Figure 6**)(Fisher and Turner, 2007; Etchells
406 and Turner, 2010; Wang et al., 2018). These mutants are also characterised by reductions in
407 vascular cell number (Hirakawa et al., 2008). To investigate genetic interactions between *pxy*
408 and *lbd4*, we generated *pxy lbd4* double mutants. The gross morphology of these plants did
409 not differ from that of the *pxy* single mutants, but *lbd4* enhanced the cell division phenotype
410 of *pxy*, as *pxy lbd4* bundles had fewer cells per vascular bundle than the parental lines
411 (**Figure 6A; Supplemental Data Set 5**). We counted the number of differentiated phloem
412 cells to assess the recruitment of phloem precursors into the phloem. These numbers were
413 similar in *pxy lbd4* lines compared to *pxy* and *lbd4* single mutants but were reduced compared
414 to wild type (**Figure 6B; Supplemental Data Set 5**). *lbd4* also enhanced the defect in
415 phloem distribution along the vascular radial axis of *pxy* (**Figure 6C; red arrowheads in**

6E). Finally, the tangential:radial axis ratio of vascular bundles was higher in the *lbd4 pxy* lines relative to the controls (**Figure 6D**), demonstrating a change to overall vascular bundle shape.

Vascular organisation requires that *CLE41*/*42*/*44* generate a TDIF maximum in the phloem. Ectopic *CLE41* expression leads to intercalated xylem and phloem, presumably due to a change in the distribution of active TDIF-PXY complexes (Etchells and Turner, 2010). *LBD4* expression is elevated in response to TDIF-PXY (**Figure 4C; Supplemental Table 1**). Thus, we predicted that the defects of *IRX3:CLE41* would be attenuated in the absence of *LBD4*. Cell number within vascular bundles was unchanged in *lbd4* but significantly increased in *IRX3:CLE41* compared to the wild type (**Figure 6F,G**). Introduction of the *lbd4* mutation into *IRX3:CLE41* lines suppressed this phenotype. The tangential:radial ratio of *IRX3:CLE41 lbd4* lines was indistinguishable from that of wild type and *lbd4* (**Figure 6H**). Thus, the changes to vascular bundle shape caused by the *IRX3:CLE41* construct were dependent on *LBD4*. Intercalation of xylem and phloem was also reduced in *IRX3:CLE41 lbd4* compared to *IRX3:CLE41*. Finally, *lbd4* attenuated the gross morphological defects of *IRX3:CLE41* (**Supplemental Figure 7**). Thus, *lbd4* suppresses the *IRX3:CLE41* phenotype.

DISCUSSION

Integration of transcriptional regulators of vascular development

The study of vascular tissue development in plants has a long history. In addition to characterisation by early plant anatomists, auxin in particular was found to influence vascular formation and connectivity in the 1950s and 60s (Torrey, 1953; Sun, 1955; Sachs, 1969). In the 1990s, with the emergence of Arabidopsis as a genetic model, multiple genes were characterised as regulating vascular tissue formation (Lincoln et al., 1990; Berleth and Jurgens, 1993; Baima et al., 1995; Zhong et al., 1997; Gälweiler et al., 1998), and such discoveries have been accelerating in the post-genomic era (Ruonala et al., 2017; Fischer et al., 2019). Recently, those taking genetic, biochemical, and mathematical approaches to studying vascular development have elegantly described how a subset of these components interact (De Rybel et al., 2014; Kondo et al., 2014; Muraro et al., 2014; Vera-Sirera et al., 2015; Mellor et al., 2016; Han et al., 2018; Miyashima et al., 2019; Smet et al., 2019). Here, we used an enhanced Y1H approach to map a network with 312 nodes and 690 interactions that describes how numerous components may come together to control the patterning and proliferation of vascular tissue (**Figure 1A**). Because we screened the promoters of

components involved in auxin perception, cytokinin perception, PXY receptors, ER receptors, and GSK3 kinases, the network can be used to identify transcription factors that integrate these signals. This set of transcription factor-promoter interactions represents PXY-mediated transcriptional regulation, as perturbations in the TDIF-PXY signalling pathway (genes differentially expressed in *pxy* mutants and in *35S:CLE41* lines) are significantly enriched within our network (**Supplemental Figure 2**).

The TMO6-WOX14-LBD4 feed-forward loop is essential for vascular development

The power of our network as a resource for identifying novel interactions was demonstrated by characterizing the TMO6-WOX14-LBD4 feed-forward loop. We investigated the nature of this regulatory circuit using eY1H, LUC reporter assays, qRT-PCR, and genetic interaction analysis. The regulatory circuit appears to be central to vascular cell proliferation, as evidenced by the loss of 41% of vascular bundle cells in *tmo6 wox14 lbd4* lines relative to wild type (**Figure 2F**). We demonstrated that the feed-forward loop is regulated by auxin and TDIF-PXY signalling (**Figures 3F-K; 4A-D; 6; Supplemental Table 1**)(Etchells et al., 2013). Given that TMO6 has also been shown to be an integrator of cytokinin signalling (Schlereth et al., 2010; Miyashima et al., 2019; Smet et al., 2019), this circuit likely acts as an integration point for many critical developmental regulators.

The transcription of *HD-ZIP III* genes is thought to be activated by the TMO6 paralogue PEAR1 during primary patterning of the root vascular cylinder (Miyashima et al., 2019). In our eY1H assays, both PEAR1 and TMO6 bound to the promoters of *HD-ZIP III* genes *PHB*, *PHV*, and *REV* (**Figure 1A**; **Supplemental Data Set 2**). *HD-ZIP III* expression is thought to represses *PEAR1* transcription in a negative feedback loop (Miyashima et al., 2019), and PHV bound the *TMO6* promoter in our eY1H assay (**Figure 1A; Supplemental Data Set 2**). Therefore, it would be interesting to further study interactions between *HD-ZIP III* genes, *PEAR1*, and members of the feed-forward loop.

Members of the feed-forward loop may function redundantly with paralogues

Genetic redundancy, such as that uncovered by Miyashima et al. (2019), is a possible explanation for the finding that the *tmo6* mutants demonstrated no changes in *LBD4* expression (**Figure 3F**). Genetic redundancy might also explain the lack of mutant phenotypes for individual *LBD* family members. A recent genetic analysis aimed at characterising regulators of the vascular cambium in Arabidopsis roots also identified LBD4

as a putative vascular regulator (Zhang et al., 2019). *lbd1 lbd4* lines exhibited reduced vascular tissue area in roots. Since we demonstrated that *lbd4* acts redundantly with *lbd3* (**Supplemental Figure 3**), it is tempting to speculate that there may be genetic redundancy between these three paralogues.

Control of vascular bundle size and shape

TMO6, *WOX14*, and *LBD4* are jointly expressed at the phloem-procambium boundary in the vascular tissue of inflorescence stems (**Figure 3A-C**). These genes also act within a coherent type I feed-forward loop (Mangan and Alon, 2003), as all are positive transcriptional activators. WOX14 was sufficient to activate *TMO6* expression in wild tobacco protoplasts (**Supplemental Figure 5**) and was also required for normal expression of *TMO6* in Arabidopsis stems (**Figure 3D**). WOX14 activated *LBD4* reporter expression in wild tobacco protoplasts when co-expressed with TMO6 (**Supplemental Figure 5A**). Both WOX14 and TMO6 were required for the very highest levels of *LBD4* expression in wild tobacco (**Supplemental Figure 5A**). Such synergism may also explain why *tmo6* mutants alone did not demonstrate changes to *LBD4* expression, but *px*f *tmo6* (where WOX14 expression is reduced) and *wox4 wox14 tmo6* lines did (**Figure 3F**).

WOX genes and their targets are crucial for regulating stem cell fate in plant meristems (Laux et al., 1996; Sarkar et al., 2007; Ji et al., 2010; Etchells et al., 2013), but the roles of direct *WOX* targets in the vascular stem cell niche have been unclear. Modelling of transcriptome data in Zhang et al. (2019) also placed *WOX14* upstream of *LBD4*. The data presented here provide additional support for this interaction (**Figures 1B, 3D-F, Supplemental Figure 5**).

Organ boundaries are marked by members of the *LBD* family

Members of the *LBD*/*AS2* gene family (Iwakawa et al., 2002; Shuai et al., 2002) regulate the formation of organ boundaries during lateral root formation (Okushima et al., 2007) and at the shoot apex (Bell et al., 2012) in Arabidopsis. In hybrid poplar (*Populus tremula* × *Populus alba*), the overexpression of *PtaLBD1* increases secondary phloem production (Yordanov et al., 2010). Here, we determined that *LBD4* is expressed at the phloem-procambium boundary (**Figure 3A**). An increase in vascular bundle cell number was observed in *lbd4 SUC2:LBD4* lines, where *LBD4* expression was shifted to the phloem. Increases in cell number were restricted to the procambium and phloem. Strikingly, no change in the number of xylem cells was observed (**Figure 5D**). These data suggest that

LBD4 controls phloem cell recruitment in a spatially restricted manner (**Figure 5A,B,E**). The loss of normal xylem differentiation in *lbd4 IRX3:LBD4* bundles where *LBD4* expression was shifted to the xylem (**Figure 5C**) suggests that this occurs in part by excluding xylem identity from the phloem side of the procambium. *LBD4* could mark the phloem-procambium boundary via regulation by TDIF-PXY, WOX14, and TMO6. Notably, *TMO6* and its paralogues are thought to define the zone of procambial activity in the root (Miyashima et al., 2019). The definition of the procambium domain could be considered to include marking its edges. Thus, *LBD4* could act as a boundary regulator or as an amplifier of divisions on the phloem side of the procambium. These putative functions are not necessarily mutually exclusive.

TDIF-PXY and LBD4

pxy mutants are characterised by intercalation of xylem and phloem (Fisher and Turner, 2007). For such phenotypes to occur, boundary specification must be disrupted. In *pxy lbd4* mutants, the positions of tissues were altered because phloem was distributed differently along the radial axis of the stem (**Figure 6C**) and bundle shape was altered (**Figure 6D**). *lbd4 pxy* plants also demonstrated reductions in vascular cell division (**Figure 6A-B**). PXY-regulated vascular organisation is dependent on *CLE41* acting as a phloem-derived positional cue. Dramatic vascular reorganisation occurs when *CLE41* is expressed from the xylem in *IRX3:CLE41* lines because the position of active TDIF-PXY complexes is altered (Etchells and Turner, 2010). In turn, this leads to changes in the positions of xylem, phloem, and procambium **(Figure 6F**) and as such, these tissues are found in ectopic positions relative to wild type. Consequently, boundaries between the phloem and procambium must also be present in ectopic positions in *IRX3:CLE41*. Our observation that the *IRX3:CLE41* phenotype was strongly suppressed by *lbd4* supports the hypothesis that *LBD4* marks the phloem-procambium boundary, since in *lbd4 IRX3:CLE41* plants, phloem was restored to the position it occupied in the wild type (**Figure 6F**). Therefore, the putative ectopic *LBD4*-specified boundary tissue observed in *IRX3:CLE41* lines was removed in these plants.

In conclusion, a genetic interaction between *LBD4* and *PXY* regulates vascular bundle shape. *LBD4* also determines stem cell number in the vascular meristem via regulation by *TMO6* and *WOX14* and redundantly with *LBD3*. Our PXY-mediated transcriptional network provides a framework for exploring other interacting regulators at the transcriptional level.

METHODS

552 **Gene expression analysis**

553 Microarray analysis was used to compare the transcriptomes of *Arabidopsis thaliana* Col-0
554 and *35S:CLE41*; the experimental set up, preparation of total RNA, synthesis of biotinalated
555 cDNA, subsequent hybridization to ATH1 Affymetrix GeneChip oligonucleotide arrays, and
556 detection were described previously (Etchells et al., 2012). Briefly, following germination on
557 MS agar plates, plants were transferred to soil and grown under long-day conditions (see
558 below) for 5 weeks. Inflorescence stems were harvested, stripped of side branches, and
559 divided into four sections of equal size. RNA was isolated from the third section from the top
560 using TRIzol (Invitrogen). Samples were prepared in triplicate for each genotype, and
561 following RNA extraction, processing was carried out at the University of Manchester
562 Genomic Technologies Facility
563 (http://www.ls.manchester.ac.uk/research/facilities/microarray/). Technical QC was
564 performed as described (Li and Wong, 2001), and background correction, normalization, and
565 gene expression analysis were performed using RMA in Bioconductor (Bolstad et al., 2003).
566 Differential expression analysis was performed using Limma (Smyth, 2004). No probe is
567 present for the *WOX4* gene on this microarray chip.
568
569 Gene expression in inflorescence stems was compared by quantitative RT-PCR using RNA
570 isolated with TRIzol reagent (Life Technologies). Samples were measured in technical
571 triplicates (reactions per sample) on biological triplicates (independent samples per genotype
572 and/or treatment). The RNA was DNase treated with RQ1 (Promega) prior to cDNA
573 synthesis using a poly-T primer and BioScript reverse transcriptase (Bioline). qPCRBIO
574 SyGreen Mix (PCR Biosystems) and primers described in **Supplemental Data Set 6** were
575 used with a CFX Connect machine (BioRad). Relative expression was determined using a
576 comparative threshold cycle (Ct) method using average amplification efficiency for each
577 primer pair, as determined using LinReg (Ramakers et al., 2003). Samples were normalised
578 to 18S rRNA (not shown) and *ACT2* (shown). Results were similar regardless of the control
579 used.
580
581 To characterize changes in gene expression in response to TDIF and P9A peptides, or IAA
582 application, seeds were stratified prior to incubation in a Sanyo MLR-351H plant growth
583 chamber set to 23°C and constant light on ½× MS with 1% agar. At 5 days, seedlings were
584 transferred to liquid ½ × MS medium containing either 5 μM TDIF (His-Glu-Val-Hyp-Ser-
585 Gly-Hyp-Asn-Pro-Ile-Ser-Asn) or negative control P9A (His-Glu-Val-Hyp-Ser-Gly-Hyp-

586 Asn-Ala-Ile-Ser-Asn; Bachem, Switzerland), or 10 μM IAA. Plants were maintained on a
587 rocking platform for 1 hour, snap frozen in liquid nitrogen, and subjected to RNA extraction
588 and qRT-PCR analysis as described above.
589
590 **eY1H assays**
591 Yeast cells were grown using standard methods (Brady et al., 2011; Gaudinier et al., 2011;
592 Reece-Hoyes et al., 2011; Taylor-Teeples et al., 2015). Briefly, YPDA medium was used for
593 unrestrained growth. -Trp, -His-Ura, or -His-Ura-Trp (containing 3AT when necessary)
594 medium was used apply selection. The transcription factor library contained 812 unique
595 cDNAs fused to the GAL4 activation domain in pDEST-AD-2μ, which are maintained as
596 plasmids in yeast and enable growth on -Trp medium. For promoter clones, promoter
597 fragments (1.2-3.5 kb) were amplified using LA taq (Takara) and cloned using 5'TOPO (Life
598 Technologies). These entry clones were used to create reporter constructs via Gateway
599 recombination. The use of pMW2 clones enabled selection on –His medium and detection of
600 interactions via growth on plates supplemented with 3AT. pMW3 (selection on -Ura
601 medium) contained a LacZ reporter. Both vectors were transformed into yeast strain
602 YM4271, integrated into the yeast genome via homologous recombination, and selected on -
603 His -Ura plates. Colonies with no autoactivation in X-gal that grew on moderate 3AT
604 concentrations (10-100 mM) were selected. The presence of both reporters was confirmed by
605 PCR.
606
607 eY1H was performed as described (Gaudinier et al., 2011; Reece-Hoyes et al., 2011) using a
608 RotoR HD robot (Singer). Briefly, mating was carried out by combining yeast cells
609 containing the transcription factor and promoter constructs on a YPDA plate. After diploid
610 selection using -His -Ura -Trp plates, the diploids were plated onto plates supplemented with
611 3AT, and onto YPDA plates containing a nitrocellulose filter. Following two days of growth
612 at room temperature, the nitrocellulose filters were subjected to an X-gal assay. For 3AT
613 plates, the plates were checked daily for colonies with increased growth. A network was
614 subsequently constructed by importing the directional interactions into Cytoscape.
615
616 **Testing transcription factor-promoter interactions**
617 To test transcription factor-promoter interactions using a dual luciferase assay system, target
618 promoters were cloned upstream of the *LUC* reporter gene in pGreenII-0800-LUC, which
619 also contained a *35S:REN* control cassette. Transcription factor sequences were cloned

behind the *35S* promoter in pGreenII 62-SK (Hellens et al., 2005). A ClonExpress II One Step Cloning Kit (Vazyme), and primers listed in **Supplemental Data Set 6** was used for vector construction. Reporter detection was performed using the Dual-Luciferase Reporter Assay System (Promega). Boxplots in **Supplemental Figure 5** show data from four biological replicates.

Wild tobacco leaf protoplasts were generated by immersing leaf material in a solution containing 1.5% CellulaseR10 (Yakult), 0.2–0.4% MacerozymeR10 (Yakult), 1% HemiCellulase (sigma), 0.4 M mannitol, 20 mM KCl, 20 mM MES (pH 5.7), 10 mM $CaCl_2$, 0.1% BSA for 12 h. An equal volume of W5 solution (150 mM NaCl, 125 mM $CaCl_2$, 5 mM KCl, 2 mM MES [pH 5.7]) was added prior to passing the mixture through a 200-mesh sieve. Protoplasts were collected by centrifugation and resuspended in ice-cold W5 (Duarte et al., 2016). Purified plasmids were transferred into these cells using the PEG–calcium method with minor modifications (Yoo et al., 2007).

Generation of plant stocks

Seeds were stratified for 2 d at 4°C in 0.1% agar prior to sowing on a mix of 75% Levington F2 compost or on Murashige and Skoog (MS) medium, 1% agar (w/v) on vertical plates. Plants were grown at 22°C under long-day conditions (16 h light/8 h dark, 300 µmol m−2 s−1, provided by cool-white fluorescent bulbs, supplemented with incandescent lighting).

Seed lines were all in the Col-0 background. *35S:CLE41*, *pxy-3*, *wox4*, *wox14*, *IRX3:CLE41*, *IRX3:CLE41 wox4*, *px*f (*pxy pxl1 pxl2*) have been described previously (Fisher and Turner, 2007; Etchells and Turner, 2010; Hirakawa et al., 2010; Etchells et al., 2013)(**Supplemental Table 4**). *lbd3* (WiscDsLoxHs070_10G) (Woody et al., 2007) and *lbd4* (Salk_146141) (Alonso et al., 2003) mutant lines (**Supplemental Table 4**) were identified using the TAIR database (Swarbreck et al., 2008) and confirmed using PCR. The *lbd4* allele harboured the T-DNA insertion in the *LBD4* 5' UTR, and we could not detect *LBD4* mRNA using qRT-PCR. *pxy lbd4*, *lbd3 lbd4*, *wox4 lbd4* and *IRX3:CLE41 lbd4* lines were identified in segregating F2 populations by PCR. *tmo6* lines (**Supplemental Table 4**) were generated by genome editing (Xing et al., 2014; Wang et al., 2015). Target sequences AAGAAACCTTCTCCTGCAA and CTCTAAGGAACATCCCCGTG were identified using CRISPR-PLANT (Xie et al., 2014) and tested for off-targets (Bae et al., 2014). Primers incorporating the target sequences (**Supplemental Data Set 6** were used in a PCR with plasmid pCBC-DT1T2 as template to generate a PCR product with a *TMO6* guide RNA, which was in turn incorporated into

pHEE2E-TRI using a Golden Gate reaction. The resulting *TMO6* CRISPR/Cas9 clone was transferred to Arabidopsis by the floral dip method (Clough and Bent, 1998). Mutants were selected with primers that flanked the guide RNA target sites (**Supplemental Figure 8**). Oligonucleotides used for genotyping are described in **Supplemental Data Set 6**.

The CRISPR construct used to generate the *cle41,42,43,44* (*tdif*) mutant was built using the *pCUT* vector system (Peterson et al., 2016). For each of the four targeted CLE genes, a 20 bp gRNA target site was selected upstream of the dodecapeptide coding region in the genomic sequence. A gRNA gene array was synthesized by GeneArt (Thermo Fisher) as a group of four *AtU6:gRNA* tandem constructs, which was subsequently cloned into the *pCUT4* binary vector via restriction enzyme digestion methods as previously described (Peterson et al., 2016). Col-0 plants were transformed with the CRISPR binary construct via the floral dip method and T1 transgenic seed derived was selected on B5 medium without sucrose and containing 100 mg/L hygromycin. The T1 generation was screened for editing efficiency by sequencing the CLE gene PCR products amplified from leaf DNA. Plants confirmed to have efficient editing had overlapping sequence traces originating at the -3 position from the PAM. T2 seed derived from plants with efficient editing was grown on selective B5 medium, DNA was collected, and each of the four *CLE* target genes was amplified via PCR. The products were sequenced directly via Sanger sequencing using primers listed in Supplemental Data Set 6. These plants demonstrated a *pxy*-like phenotype, which was partially recoverable by transformation with a *SUC2:CLE41* construct (**Supplemental Figure 6**) that was described previously (Etchells and Turner, 2010).

The *wox14 lbd4 tmo6* lines and respective double mutants were identified in F2 and F3 populations. *IRX3:LBD4* and *SUC2:LBD4* lines were generated by PCR amplification of a genomic fragment incorporating the *LBD4* coding region, which was cloned into pENTR-D-TOPO prior to transfer into plasmid p3KC (Atanassov et al., 2009). For *SUC2:LBD4*, the *IRX3* promoter in p3KC was replaced with that of *SUC2*. The resulting over-expression clone was introduced into Arabidopsis using the floral dip method (Clough and Bent, 1998).

Histology

Plant vascular tissue visualisation was carried out in 4 μm resin sections stained with 0.05% aqueous toluidine blue, following fixation of plant material in FAA, dehydration through an ethanol series, and embedding in JB4 resin. Alternatively, hand sections were stained with

500 mM aniline blue dissolved in 100 mM phosphate buffer, pH 7.2 and viewed under a UV lamp.

Accession numbers

The accession numbers of the factors central to this paper are CLE41 (AT3G24770), CLE42 (AT2G34925), CLE44 (AT4G13195), LBD3 (AT1G16530), LBD4 (AT1G31320), PXL1 (AT1G08590), PXL2 (AT4G28650), PXY (AT5G61480), TMO6 (AT5G60200), WOX4 (AT1G46480), and WOX14 (AT1G20700). For a comprehensive list of accession numbers represented in the eY1H data, please see **Supplemental Data Set 2**.

Microarray data have been submitted in a MIAME compliant standard to GEO (accession number GSE123162).

Supplemental Data

Supplemental Figure 1. qRT-PCR confirmation of microarray experiment.

Supplemental Figure 2. Network of genes misexpressed in different genetic backgrounds.

Supplemental Figure 3. Vascular tissue in *lbd3 lbd4* double mutants.

Supplemental Figure 4. *In situ* controls, and *LBD4* expression along the apical-basal axis of wild type and *pxy* mutant stems

Supplemental Figure 5. *LBD4pro:LUC* expression in the presence of WOX14 and TMO6.

Supplemental Figure 6. Phenotype of *cle41 cle42 cle43 cle44* quadruple mutants.

Supplemental Figure 7. *lbd4* suppresses the *IRX3:CLE41* phenotype.

Supplemental Figure 8. Genome edited *tmo6* allele.

Supplemental Table 1. Expression of genes demonstrating expression changes in 35S:CLE41 compared to wild type in array data analysed in this study.

Supplemental Table 2. Promoters analysed using Y1H.

Supplemental Table 3. P-values for qRT-PCR analysis of *LBD4* expression differences in *px*f *tmo6* and *wox4 wox14 tmo6* mutants and controls.

Supplemental Table 4. Plant lines used in this manuscript.

Supplemental Data Set 1. Differentially expressed genes in *35S:CLE41* compared to wild type, as determined using microarrays.

Supplemental Data Set 2. Transcription factor-promoter interactions identified in eY1H.

Supplemental Data Set 3. List of interacting transcription factors and the transcription factors families that they represent.

Supplemental Data Set 4. Promoters arranged in order of those with the most to fewest interacting transcription factors.

Supplemental Data Set 5. Pairwise p-values for all comparisons of vascular phenotypes in this manuscript.

Supplemental Data Set 6. Oligonucleotides used in this study.

ACKNOWLEDGEMENTS

The authors gratefully acknowledge financial support from via a Marie Skłodowska-Curie fellowship to JPE, N8 Agrifood pump priming finds to JPE and SRT, the Jo Kolk Study Fund from the VVAO to MES. This research was supported by a National Science Foundation Plant Genome Research Program (IOS-1546837) to ZLN. SMB was partially funded through a Howard Hughes Faculty Scholar fellowship. We thank Dória de Souza-Etchells for technical assistance.

AUTHOR CONTRIBUTIONS

S.M.B., J.P.E., S.R.T., D.W., J.T.K., X.Y., H.S., Z.L.N. designed the experiments. M.E.S., S.M., H.S., C.G., A.M.B., C.L.S., A.G., C.J.W., J.T.K., and J.P.E. performed the experiments. All authors analysed the data. J.P.E. and S.M.B. drafted the manuscript.

REFERENCES

Alonso, J.M., Stepanova, A.N., Leisse, T.J., Kim, C.J., Chen, H., Shinn, P., Stevenson, D.K., Zimmerman, J., Barajas, P., Cheuk, R., Gadrinab, C., Heller, C., Jeske, A., Koesema, E., Meyers, C.C., Parker, H., Prednis, L., Ansari, Y., Choy, N., Deen, H., Geralt, M., Hazari, N., Hom, E., Karnes, M., Mulholland, C., Ndubaku, R., Schmidt, I., Guzman, P., Aguilar-Henonin, L., Schmid, M., Weigel, D., Carter, D.E., Marchand, T., Risseeuw, E., Brogden, D., Zeko, A., Crosby, W.L., Berry, C.C., and Ecker, J.R. (2003). Genome-Wide Insertional Mutagenesis of Arabidopsis thaliana. Science **301,** 653-657.

Atanassov, I., Atanassov, I., Etchells, J.P., and Turner, S. (2009). A simple, flexible and efficient PCR-fusion/Gateway cloning procedure for gene fusion, site-directed mutagenesis, short sequence insertion and domain deletions and swaps. Plant Methods **5,** 14.

753 **Bae, S., Park, J., and Kim, J.-S.** (2014). Cas-OFFinder: a fast and versatile algorithm that
754 searches for potential off-target sites of Cas9 RNA-guided endonucleases.
755 Bioinformatics **30,** 1473-1475.
756 **Baima, S., Nobili, F., Sessa, G., Lucchetti, S., Ruberti, I., and Morelli, G.** (1995). The
757 expression of the Athb-8 homeobox gene is restricted to provascular cells in
758 Arabidopsis thaliana. Development **121,** 4171-4182.
759 **Baima, S., Possenti, M., Matteucci, A., Wisman, E., Altamura, M.M., Ruberti, I., and**
760 **Morelli, G.** (2001). The Arabidopsis ATHB-8 HD-Zip Protein Acts as a
761 Differentiation-Promoting Transcription Factor of the Vascular Meristems. Plant
762 Physiology **126,** 643-655.
763 **Baima, S., Forte, V., Possenti, M., Peñalosa, A., Leoni, G., Salvi, S., Felici, B., Ruberti,**
764 **I., and Morelli, G.** (2014). Negative feedback regulation of auxin signaling by
765 ATHB8/ACL5-BUD2 transcription module. Molecular plant **7,** 1006-1025.
766 **Bell, E.M., Lin, W.-c., Husbands, A.Y., Yu, L., Jaganatha, V., Jablonska, B., Mangeon,**
767 **A., Neff, M.M., Girke, T., and Springer, P.S.** (2012). Arabidopsis LATERAL
768 ORGAN BOUNDARIES negatively regulates brassinosteroid accumulation to limit
769 growth in organ boundaries. Proceedings of the National Academy of Sciences **109,**
770 21146-21151.
771 **Berleth, T., and Jurgens, G.** (1993). The role of the monopteros gene in organising the basal
772 body region of the Arabidopsis embryo. Development **118,** 575-587.
773 **Bolstad, B.M., Irizarry, R.A., Astrand, M., and Speed, T.P.** (2003). A comparison of
774 normalization methods for high density oligonucleotide array data based on variance
775 and bias. Bioinformatics **19,** 185-193.
776 **Brackmann, K., Qi, J., Gebert, M., Jouannet, V., Schlamp, T., Grünwald, K., Wallner,**
777 **E.-S., Novikova, D.D., Levitsky, V.G., Agustí, J., Sanchez, P., Lohmann, J.U.,**
778 **and Greb, T.** (2018). Spatial specificity of auxin responses coordinates wood
779 formation. Nature Communications **9,** 875.
780 **Brady, S.M., Zhang, L., Megraw, M., Martinez, N.J., Jiang, E., Yi, C.S., Liu, W., Zeng,**
781 **A., Taylor-Teeples, M., Kim, D., Ahnert, S., Ohler, U., Ware, D., Walhout,**
782 **A.J.M., and Benfey, P.N.** (2011). A stele-enriched gene regulatory network in the
783 Arabidopsis root. Mol Syst Biol **7**.
784 **Cano-Delgado, A., Yin, Y.H., Yu, C., Vafeados, D., Mora-Garcia, S., Cheng, J.C., Nam,**
785 **K.H., Li, J.M., and Chory, J.** (2004). BRL1 and BRL3 are novel brassinosteroid

receptors that function in vascular differentiation in Arabidopsis. Development **131,** 5341-5351.

Carlsbecker, A., Lee, J.-Y., Roberts, C.J., Dettmer, J., Lehesranta, S., Zhou, J., Lindgren, O., Moreno-Risueno, M.A., Vatén, A., Thitamadee, S., Campilho, A., Sebastian, J., Bowman, J.L., Helariutta, Y., and Benfey, P.N. (2010). Cell signalling by microRNA165/6 directs gene dose-dependent root cell fate. Nature **465,** 316-321.

Chen, M.-K., Wilson, R.L., Palme, K., Ditengou, F.A., and Shpak, E.D. (2013). ERECTA Family Genes Regulate Auxin Transport in the Shoot Apical Meristem and Forming Leaf Primordia. Plant Physiology **162,** 1978-1991.

Cho, H., Ryu, H., Rho, S., Hill, K., Smith, S., Audenaert, D., Park, J., Han, S., Beeckman, T., Bennett, M.J., Hwang, D., De Smet, I., and Hwang, I. (2014). A secreted peptide acts on BIN2-mediated phosphorylation of ARFs to potentiate auxin response during lateral root development. Nat Cell Biol **16,** 66-76.

Clough, S.J., and Bent, A.F. (1998). Floral dip: a simplified method for Agrobacterium-mediated transformation of Arabidopsis thaliana. Plant Journal **16,** 735-743.

De Rybel, B., Möller, B., Yoshida, S., Grabowicz, I., Barbier de Reuille, P., Boeren, S., Smith, R.S., Borst, J.W., and Weijers, D. (2013). A bHLH Complex Controls Embryonic Vascular Tissue Establishment and Indeterminate Growth in Arabidopsis. Developmental cell.

De Rybel, B., Adibi, M., Breda, A.S., Wendrich, J.R., Smit, M.E., Novák, O., Yamaguchi, N., Yoshida, S., Van Isterdael, G., Palovaara, J., Nijsse, B., Boekschoten, M.V., Hooiveld, G., Beeckman, T., Wagner, D., Ljung, K., Fleck, C., and Weijers, D. (2014). Integration of growth and patterning during vascular tissue formation in Arabidopsis. Science (New York, N.Y.) **345,** 1255215-1255215.

Duarte, P., Ribeiro, D., Carqueijeiro, I., Bettencourt, S., and Sottomayor, M. (2016). Protoplast Transformation as a Plant-Transferable Transient Expression System. In Biotechnology of Plant Secondary Metabolism: Methods and Protocols, A.G. Fett-Neto, ed (New York, NY: Springer New York), pp. 137-148.

Emery, J.F., Floyd, S.K., Alvarez, J., Eshed, Y., Hawker, N.P., Izhaki, A., Baum, S.F., and Bowman, J.L. (2003). Radial Patterning of *Arabidopsis* Shoots by Class III HD-ZIP and KANADI Genes. Current Biology **13,** 1768-1774.

Etchells, J.P., and Turner, S.R. (2010). The PXY-CLE41 receptor ligand pair defines a multifunctional pathway that controls the rate and orientation of vascular cell division. Development **137,** 767-774.

Etchells, J.P., Provost, C.M., and Turner, S.R. (2012). Plant Vascular Cell Division Is Maintained by an Interaction between PXY and Ethylene Signalling. PLoS Genetics **8,** e1002997.

Etchells, J.P., Provost, C.M., Mishra, L., and Turner, S.R. (2013). *WOX4* and *WOX14* act downstream of the PXY receptor kinase to regulate plant vascular proliferation independently of any role in vascular organisation. Development **140,** 2224-2234.

Fischer, U., Kucukoglu, M., Helariutta, Y., and Bhalerao, R.P. (2019). The Dynamics of Cambial Stem Cell Activity **70,** null.

Fisher, K., and Turner, S. (2007). PXY, a receptor-like kinase essential for maintaining polarity during plant vascular-tissue development. Current Biology **17,** 1061-1066.

Gälweiler, L., Guan, C., Müller, A., Wisman, E., Mendgen, K., Yephremov, A., and Palme, K. (1998). Regulation of Polar Auxin Transport by AtPIN1 in Arabidopsis Vascular Tissue. Science **282,** 2226-2230.

Gaudinier, A., Tang, M., Bagman, A.M., and Brady, S.M. (2017). Identification of Protein-DNA Interactions Using Enhanced Yeast One-Hybrid Assays and a Semiautomated Approach. Methods Mol Biol **1610,** 187-215.

Gaudinier, A., Zhang, L., Reece-Hoyes, J.S., Taylor-Teeples, M., Pu, L., Liu, Z., Breton, G., Pruneda-Paz, J.L., Kim, D., Kay, S.A., Walhout, A.J.M., Ware, D., and Brady, S.M. (2011). Enhanced Y1H assays for Arabidopsis. Nat Meth **8,** 1053-1055.

Guo, Y., Qin, G., Gu, H., and Qu, L.-J. (2009). Dof5.6/HCA2, a Dof Transcription Factor Gene, Regulates Interfascicular Cambium Formation and Vascular Tissue Development in Arabidopsis. The Plant Cell**,** tpc.108.064139.

Han, S., Cho, H., Noh, J., Qi, J., Jung, H.-J., Nam, H., Lee, S., Hwang, D., Greb, T., and Hwang, I. (2018). BIL1-mediated MP phosphorylation integrates PXY and cytokinin signalling in secondary growth. Nature Plants.

Hardtke, C.S., and Berleth, T. (1998). The Arabidopsis gene MONOPTEROS encodes a transcription factor mediating embryo axis formation and vascular development. Embo Journal **17,** 1405-1411.

He, J.-X., Gendron, J.M., Yang, Y., Li, J., and Wang, Z.-Y. (2002). The GSK3-like kinase BIN2 phosphorylates and destabilizes BZR1, a positive regulator of the

brassinosteroid signaling pathway in Arabidopsis. Proceedings of the National Academy of Sciences **99,** 10185-10190.

Hellens, R.P., Allan, A.C., Friel, E.N., Bolitho, K., Grafton, K., Templeton, M.D., Karunairetnam, S., Gleave, A.P., and Laing, W.A.J.P.M. (2005). Transient expression vectors for functional genomics, quantification of promoter activity and RNA silencing in plants **1,** 13.

Hirakawa, Y., Kondo, Y., and Fukuda, H. (2010). TDIF Peptide Signaling Regulates Vascular Stem Cell Proliferation via the WOX4 Homeobox Gene in Arabidopsis. Plant Cell **22,** 2618-2629.

Hirakawa, Y., Shinohara, H., Kondo, Y., Inoue, A., Nakanomyo, I., Ogawa, M., Sawa, S., Ohashi-Ito, K., Matsubayashi, Y., and Fukuda, H. (2008). Non-cell-autonomous control of vascular stem cell fate by a CLE peptide/receptor system. Proceedings of the National Academy of Sciences, USA **105,** 15208-15213.

Ikematsu, S., Tasaka, M., Torii, K.U., and Uchida, N. (2017). ERECTA-family receptor kinase genes redundantly prevent premature progression of secondary growth in the Arabidopsis hypocotyl. New Phytologist **213,** 1697-1709.

Ito, Y., Nakanomyo, I., Motose, H., Iwamoto, K., Sawa, S., Dohmae, N., and Fukuda, H. (2006). Dodeca-CLE peptides as suppressors of plant stem cell differentiation. Science **313,** 842-845.

Iwakawa, H., Ueno, Y., Semiarti, E., Onouchi, H., Kojima, S., Tsukaya, H., Hasebe, M., Soma, T., Ikezaki, M., Machida, C., and Machida, Y. (2002). The *ASYMMETRIC LEAVES 2* gene of *Arabidopsis thaliana*, required for foramation of a symmetric flat leaf lamina, encodes a member of a novel family of proteins characterised by cystein repeats and a leucine zipper. Plant and Cell Physiology **43,** 467-478.

Ji, J., Strable, J., Shimizu, R., Koenig, D., Sinha, N., and Scanlon, M.J. (2010). WOX4 Promotes Procambial Development. Plant Physiology **152,** 1346-1356.

Kalir, S., Mangan, S., and Alon, U. (2005). A coherent feed□forward loop with a SUM input function prolongs flagella expression in Escherichia coli **1,** 2005.0006.

Kaplan, S., Bren, A., Dekel, E., and Alon, U. (2008). The incoherent feed□forward loop can generate non□monotonic input functions for genes **4,** 203.

Kim, T.-W., Michniewicz, M., Bergmann, D.C., and Wang, Z.-Y. (2012). Brassinosteroid regulates stomatal development by GSK3-mediated inhibition of a MAPK pathway. Nature **482,** 419.

Kondo, Y., Ito, T., Nakagami, H., Hirakawa, Y., Saito, M., Tamaki, T., Shirasu, K., and Fukuda, H. (2014). Plant GSK3 proteins regulate xylem cell differentiation downstream of TDIF–TDR signalling. Nat Commun **5**.

Konishi, M., Donner, T.J., Scarpella, E., and Yanagisawa, S. (2015). MONOPTEROS directly activates the auxin-inducible promoter of the Dof5.8 transcription factor gene in Arabidopsis thaliana leaf provascular cells. Journal of Experimental Botany **66,** 283-291.

Laux, T., Mayer, K.F., Berger, J., and Jurgens, G. (1996). The WUSCHEL gene is required for shoot and floral meristem integrity in Arabidopsis. Development **122,** 87-96.

Le Hir, R., and Bellini, C. (2013). The Plant-Specific Dof Transcription Factors Family: New Players Involved in Vascular System Development and Functioning in Arabidopsis. Frontiers in Plant Science **4**.

Li, C., and Wong, W.H. (2001). Model-based analysis of oligonucleotide arrays: Expression index computation and outlier detection. Proceedings of the National Academy of Sciences, USA **98,** 31-36.

Lincoln, C., Britton, J.H., and Estelle, M. (1990). Growth and development of the axr1 mutants of Arabidopsis **2,** 1071-1080.

Mangan, S., and Alon, U. (2003). Structure and function of the feed-forward loop network motif. Proceedings of the National Academy of Sciences **100,** 11980-11985.

Mattsson, J., Ckurshumova, W., and Berleth, T. (2003). Auxin signaling in Arabidopsis leaf vascular development. Plant physiology **131,** 1327-1339.

McConnell, J.R., Emery, J., Eshed, Y., Bao, N., Bowman, J., and Barton, M.K. (2001). Role of *PHABULOSA* and *PHAVOLUTA* in determining radial patterning in shoots. Nature **411,** 709-713.

Mellor, N., Adibi, M., El-Showk, S., De Rybel, B., King, J., Mähönen, A.P., Weijers, D., and Bishopp, A. (2016). Theoretical approaches to understanding root vascular patterning: a consensus between recent models. Journal of Experimental Botany.

Miyashima, S., Roszak, P., Sevilem, I., Toyokura, K., Blob, B., Heo, J.-o., Mellor, N., Help-Rinta-Rahko, H., Otero, S., Smet, W., Boekschoten, M., Hooiveld, G., Hashimoto, K., Smetana, O., Siligato, R., Wallner, E.-S., Mähönen, A.P., Kondo, Y., Melnyk, C.W., Greb, T., Nakajima, K., Sozzani, R., Bishopp, A., De Rybel, B., and Helariutta, Y. (2019). Mobile PEAR transcription factors integrate positional cues to prime cambial growth. Nature.

Morita, J., Kato, K., Nakane, T., Kondo, Y., Fukuda, H., Nishimasu, H., Ishitani, R., and Nureki, O. (2016). Crystal structure of the plant receptor-like kinase TDR in complex with the TDIF peptide. Nature Communications **7,** 12383.

Müller, C.J., Valdés, A.E., Wang, G., Ramachandran, P., Beste, L., Uddenberg, D., and Carlsbecker, A. (2016). PHABULOSA Mediates an Auxin Signaling Loop to Regulate Vascular Patterning in Arabidopsis. Plant physiology **170,** 956-970.

Muraro, D., Mellor, N., Pound, M.P., Help, H., Lucas, M., Chopard, J., Byrne, H.M., Godin, C., Hodgman, T.C., King, J.R., Pridmore, T.P., Helariutta, Y., Bennett, M.J., and Bishopp, A. (2014). Integration of hormonal signaling networks and mobile microRNAs is required for vascular patterning in Arabidopsis roots. PNAS **111,** 857-862.

Ohashi-Ito, K., and Bergmann, D.C. (2007). Regulation of the Arabidopsis root vascular initial population by LONESOME HIGHWAY. Development **134,** 2959-2968.

Ohashi-Ito, K., Saegusa, M., Iwamoto, K., Oda, Y., Katayama, H., Kojima, M., Sakakibara, H., and Fukuda, H. (2014). A bHLH complex activates vascular cell division via cytokinin action in root apical meristem. Current biology : CB **24,** 2053-2058.

Okushima, Y., Fukaki, H., Onoda, M., Theologis, A., and Tasaka, M. (2007). ARF7 and ARF19 Regulate Lateral Root Formation via Direct Activation of LBD/ASL Genes in Arabidopsis. The Plant Cell **19,** 118-130.

Peterson, B.A., Haak, D.C., Nishimura, M.T., Teixeira, P.J.P.L., James, S.R., Dangl, J.L., and Nimchuk, Z.L. (2016). Genome-Wide Assessment of Efficiency and Specificity in CRISPR/Cas9 Mediated Multiple Site Targeting in Arabidopsis. PLOS ONE **11,** e0162169.

Prigge, M.J., Otsuga, D., Alonso, J.M., Ecker, J.R., Drews, G.N., and Clark, S.E. (2005). Class III homeodomain-leucine zipper gene family members have overlapping, antagonistic, and distinct roles in Arabidopsis development. Plant Cell **17,** 61-76.

Ragni, L., Nieminen, K., Pacheco-Villalobos, D., Sibout, R., Schwechheimer, C., and Hardtke, C.S. (2011). Mobile Gibberellin Directly Stimulates Arabidopsis Hypocotyl Xylem Expansion. Plant Cell **23,** 1322-1336.

Ramachandran, P., Carlsbecker, A., and Etchells, J.P. (2016). Class III HD-ZIPs govern vascular cell fate: an HD view on patterning and differentiation. Journal of Experimental Botany.

Ramakers, C., Ruijter, J.M., Deprez, R.H.L., and Moorman, A.F.M. (2003). Assumption-free analysis of quantitative real-time polymerase chain reaction (PCR) data. Neuroscience Letters **339,** 62-66.

Reece-Hoyes, J.S., Diallo, A., Lajoie, B., Kent, A., Shrestha, S., Kadreppa, S., Pesyna, C., Dekker, J., Myers, C.L., and Walhout, A.J.M. (2011). Enhanced yeast one-hybrid assays for high-throughput gene-centered regulatory network mapping. Nature Methods **8,** 1059.

Ruonala, R., Ko, D., and Helariutta, Y. (2017). Genetic Networks in Plant Vascular Development **51,** 335-359.

Sachs, T. (1969). Polarity and the Induction of Organized Vascular Tissues. Annals of Botany **33,** 263-275.

Sarkar, A.K., Luijten, M., Miyashima, S., Lenhard, M., Hashimoto, T., Nakajima, K., Scheres, B., Heidstra, R., and Laux, T. (2007). Conserved factors regulate signalling in Arabidopsis thaliana shoot and root stem cell organizers. Nature **446,** 811-814.

Schlereth, A., Moller, B., Liu, W., Kientz, M., Flipse, J., Rademacher, E.H., Schmid, M., Jurgens, G., and Weijers, D. (2010). MONOPTEROS controls embryonic root initiation by regulating a mobile transcription factor. Nature **464,** 913-916.

Shannon, P., Markiel, A., Ozier, O., Baliga, N.S., Wang, J.T., Ramage, D., Amin, N., Schwikowski, B., and Ideker, T. (2003). Cytoscape: A Software Environment for Integrated Models of Biomolecular Interaction Networks. Genome Research **13,** 2498-2504.

Shen-Orr, S.S., Milo, R., Mangan, S., and Alon, U. (2002). Network motifs in the transcriptional regulation network of Escherichia coli. Nature Genetics **31,** 64.

Shuai, B., Reynaga-Peña, C.G., and Springer, P.S. (2002). The Lateral Organ Boundaries Gene Defines a Novel, Plant-Specific Gene Family. Plant Physiology **129,** 747-761.

Smet, W., Sevilem, I., de Luis Balaguer, M.A., Wybouw, B., Mor, E., Miyashima, S., Blob, B., Roszak, P., Jacobs, T.B., Boekschoten, M., Hooiveld, G., Sozzani, R., Helariutta, Y., and De Rybel, B. (2019). DOF2.1 Controls Cytokinin-Dependent Vascular Cell Proliferation Downstream of TMO5/LHW. Current Biology **29,** 520-529.e526.

Smetana, O., Mäkilä, R., Lyu, M., Amiryousefi, A., Sánchez Rodríguez, F., Wu, M.-F., Solé-Gil, A., Leal Gavarrón, M., Siligato, R., Miyashima, S., Roszak, P., Blomster, T., Reed, J.W., Broholm, S., and Mähönen, A.P. (2019). High levels of

auxin signalling define the stem-cell organizer of the vascular cambium. Nature **565,** 485-489.

Smyth, G.K. (2004). Linear Models and Empirical Bayes Methods for Assessing Differential Expression in Microarray Experiments. Statistical Applications in Genetics and Molecular Biology **3,** Article 3.

Suer, S., Agusti, J., Sanchez, P., Schwarz, M., and Greb, T. (2011). WOX4 Imparts Auxin Responsiveness to Cambium Cells in Arabidopsis. The Plant Cell **23,** 3247-3259.

Sun, C.N. (1955). Anomalous Structure in the Hypocotyl of Soybean Following Treatment with 2,4-Dichlorophenoxyacetic Acid **121,** 641-641.

Swarbreck, D., Wilks, C., Lamesch, P., Berardini, T.Z., Garcia-Hernandez, M., Foerster, H., Li, D., Meyer, T., Muller, R., Ploetz, L., Radenbaugh, A., Singh, S., Swing, V., Tissier, C., Zhang, P., and Huala, E. (2008). The Arabidopsis Information Resource (TAIR): gene structure and function annotation. Nucl. Acids Res. **36,** D1009-1014.

Taylor-Teeples, M., Lin, L., de Lucas, M., Turco, G., Toal, T.W., Gaudinier, A., Young, N.F., Trabucco, G.M., Veling, M.T., Lamothe, R., Handakumbura, P.P., Xiong, G., Wang, C., Corwin, J., Tsoukalas, A., Zhang, L., Ware, D., Pauly, M., Kliebenstein, D.J., Dehesh, K., Tagkopoulos, I., Breton, G., Pruneda-Paz, J.L., Ahnert, S.E., Kay, S.A., Hazen, S.P., and Brady, S.M. (2015). An Arabidopsis gene regulatory network for secondary cell wall synthesis. Nature **517,** 571-U307.

Torrey, J.G. (1953). THE EFFECT OF CERTAIN METABOLIC INHIBITORS ON VASCULAR TISSUE DIFFERENTIATION IN ISOLATED PEA ROOTS **40,** 525-533.

Uchida, N., and Tasaka, M. (2013). Regulation of plant vascular stem cells by endodermis-derived EPFL-family peptide hormones and phloem-expressed ERECTA-family receptor kinases. Journal of Experimental Botany.

Uchida, N., Lee, J.S., Horst, R.J., Lai, H.-H., Kajita, R., Kakimoto, T., Tasaka, M., and Torii, K.U. (2012). Regulation of inflorescence architecture by intertissue layer ligand–receptor communication between endodermis and phloem. Proc Natl Acad Sci USA.

Vera-Sirera, F., De Rybel, B., Úrbez, C., Kouklas, E., Pesquera, M., Álvarez-Mahecha, J.C., Minguet, E.G., Tuominen, H., Carbonell, J., Borst, J.W., Weijers, D., and Blázquez, M.A. (2015). A bHLH-Based Feedback Loop Restricts Vascular Cell Proliferation in Plants. Developmental cell **35,** 432-443.

Waki, T., Miyashima, S., Nakanishi, M., Ikeda, Y., Hashimoto, T., and Nakajima, K. (2013). A GAL4-based targeted activation tagging system in Arabidopsis thaliana. The Plant Journal **73,** 357-367.

Wang, N., Bagdassarian, K.S., Doherty, R.E., Wang, X.Y., Kroon, J.T., Wang, W., Jermyn, I.H., Turner, S.R., and Etchells, P. (2018). Paralogues of the PXY and ER receptor kinases enforce radial patterning in plant vascular tissue. bioRxiv.

Wang, N., Bagdassarian, K.S., Doherty, R.E., Kroon, J.T., Connor, K.A., Wang, X.Y., Wang, W., Jermyn, I.H., Turner, S.R., and Etchells, J.P. (2019). Organ-specific genetic interactions between paralogues of the *PXY* and *ER* receptor kinases enforce radial patterning in *Arabidopsis* vascular tissue. Development **146,** dev177105.

Wang, Z.-P., Xing, H.-L., Dong, L., Zhang, H.-Y., Han, C.-Y., Wang, X.-C., and Chen, Q.-J. (2015). Egg cell-specific promoter-controlled CRISPR/Cas9 efficiently generates homozygous mutants for multiple target genes in Arabidopsis in a single generation. Genome Biology **16,** 144.

Woodward, C., Bemis, S.M., Hill, E.J., Sawa, S., Koshiba, T., and Torii, K.U. (2005). Interaction of Auxin and ERECTA in Elaborating Arabidopsis Inflorescence Architecture Revealed by the Activation Tagging of a New Member of the YUCCA Family Putative Flavin Monooxygenases. Plant Physiology **139,** 192-203.

Woody, S., Austin-Phillips, S., Amasino, R., and Krysan, P. (2007). The WiscDsLox T-DNA collection: an arabidopsis community resource generated by using an improved high-throughput T-DNA sequencing pipeline. Journal of Plant Research **120,** 157-165.

Xing, H.-L., Dong, L., Wang, Z.-P., Zhang, H.-Y., Han, C.-Y., Liu, B., Wang, X.-C., and Chen, Q.-J. (2014). A CRISPR/Cas9 toolkit for multiplex genome editing in plants. BMC Plant Biology **14,** 327.

Yoo, S.-D., Cho, Y.-H., and Sheen, J. (2007). Arabidopsis mesophyll protoplasts: a versatile cell system for transient gene expression analysis. Nature Protocols **2,** 1565.

Yordanov, Y.S., Regan, S., and Busov, V. (2010). Members of the LATERAL ORGAN BOUNDARIES DOMAIN Transcription Factor Family Are Involved in the Regulation of Secondary Growth in Populus. The Plant Cell Online **22,** 3662-3677.

Zhang, H., Lin, X., Han, Z., Qu, L.-J., and Chai, J. (2016). Crystal structure of PXY-TDIF complex reveals a conserved recognition mechanism among CLE peptide-receptor pairs. Cell Research **26,** 543.

Zhang, J., Eswaran, G., Alonso-Serra, J., Kucukoglu, M., Xiang, J., Yang, W., Elo, A., Nieminen, K., Damén, T., Joung, J.-G., Yun, J.-Y., Lee, J.-H., Ragni, L., Barbier de Reuille, P., Ahnert, S.E., Lee, J.-Y., Mähönen, A.P., and Helariutta, Y. (2019). Transcriptional regulatory framework for vascular cambium development in Arabidopsis roots. Nature Plants **5,** 1033-1042.

Zhong, R., and Ye, Z.-H. (1999). IFL1, a Gene Regulating Interfascicular Fiber Differentiation in Arabidopsis, Encodes a Homeodomain-Leucine Zipper Protein. Plant Cell **11,** 2139-2152.

Zhong, R., Taylor, J.J., and Ye, Z.H. (1997). Disruption of Interfascicular Fiber Differentiation in an Arabidopsis Mutant. Plant Cell **9,** 2159-2170.

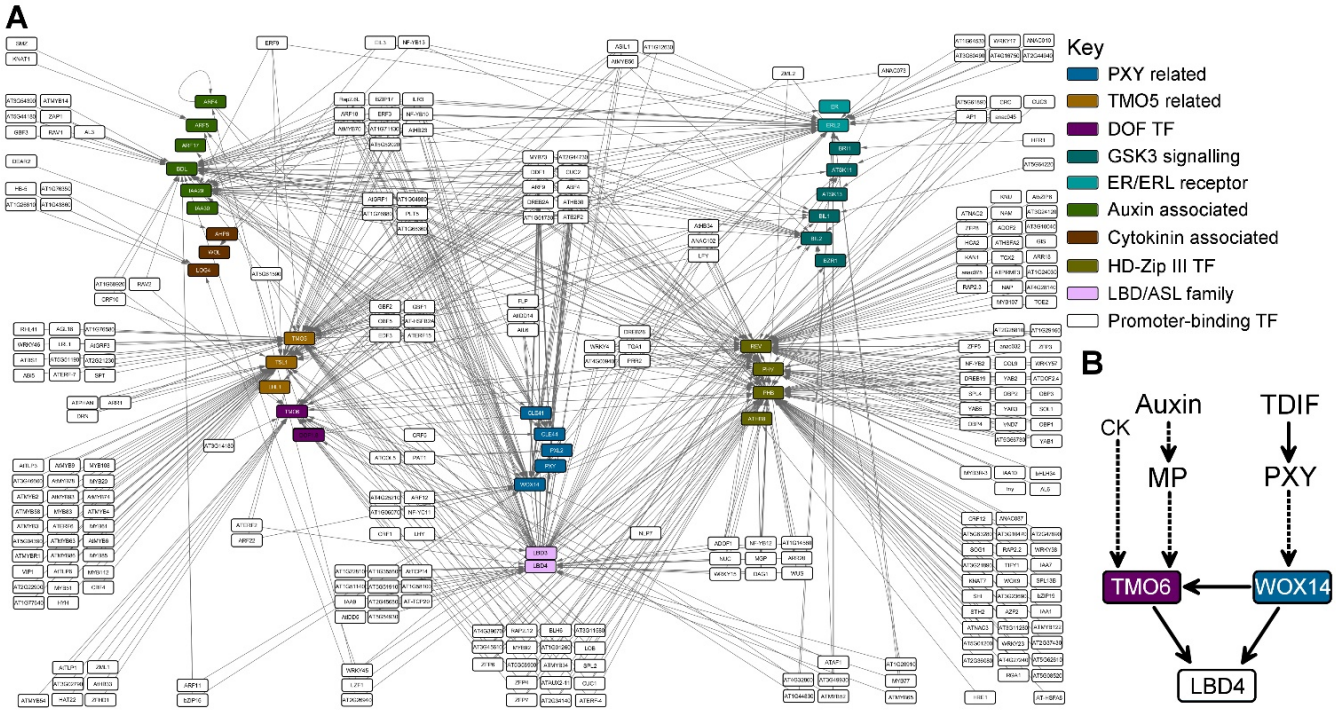

Figure 1. Diagrammatic representation of the vascular development transcriptional regulatory network

(A) Representation of all the interactions identified using eY1H. Promoters screened are shown as coloured nodes. Transcription factor are shown as white nodes. Grey lines connect transcription factor nodes, with promoter nodes representing interactions in eY1H assays. (B) Sub-network describing the feed-forward loop constituted of WOX14, TMO6 and LBD4 interactions, and its regulation by auxin, cytokinin (CK) and TDIF-PXY signalling.

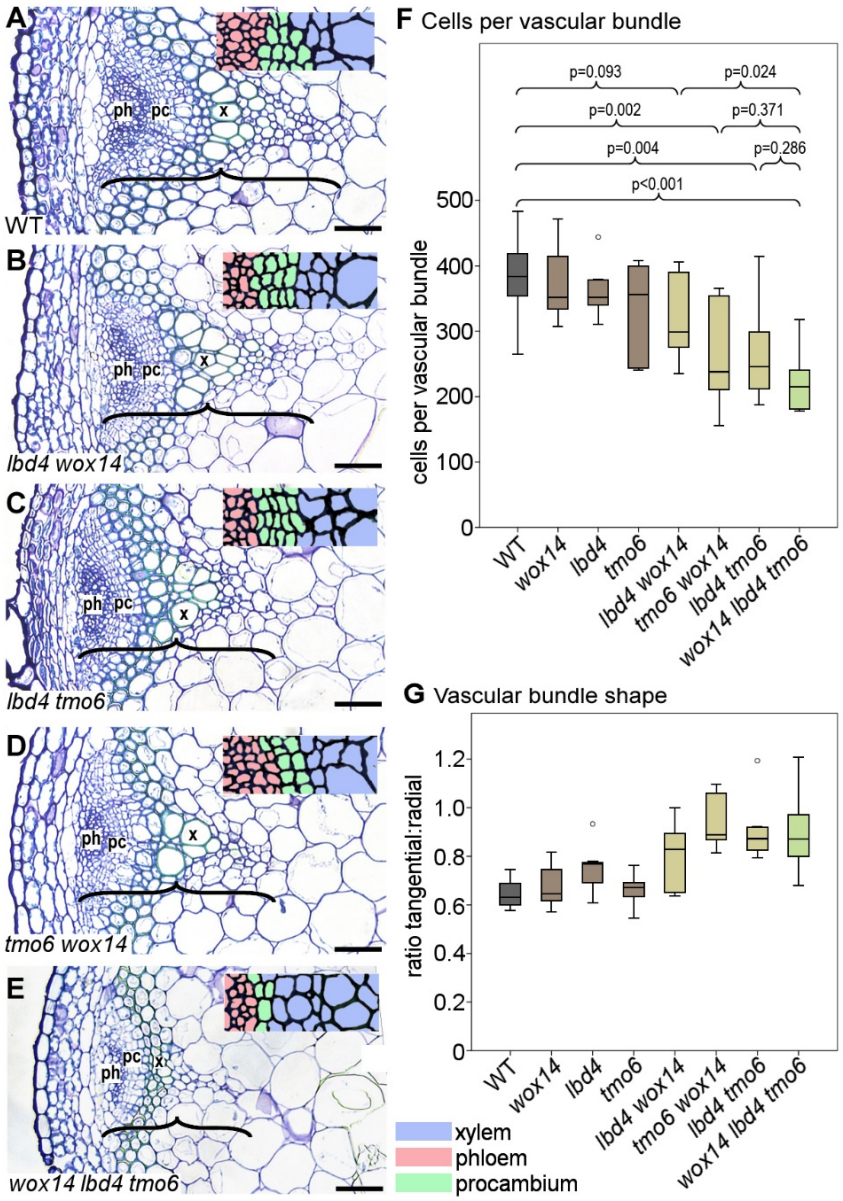

Figure 2. Consequences of removing the feed-forward loop
(A) Morphology of vascular bundles from inflorescence stems. (A) wild type, (B) *lbd4 wox14* (C) *lbd4 tmo6*, (D) *tmo6 wox14*, (E) *wox14 lbd4 tmo6*. Transverse sections were stained with toluidine blue. Insets show close-up of the cambium (green). (F) Boxplots showing mean number of cells per vascular bundle in *wox14 lbd4 tmo6*, double and single mutant controls. Significant differences were determined by ANOVA with an LSD post-hoc test (n=6). (G) Box plot showing vascular bundle shape determined by measuring the ratio of tangential to radial axis (n=6). Scale bars are 50 µm. x marks xylem, pc marks cambium, ph marks phloem, brackets mark the vascular bundle size along the radial axis of the stem. Boxplots show median (inner line) and inner quartiles (IQ, box). Whiskers extend to the highest and lowest values no greater than 1.5 times the IQ range, circles show outliers.

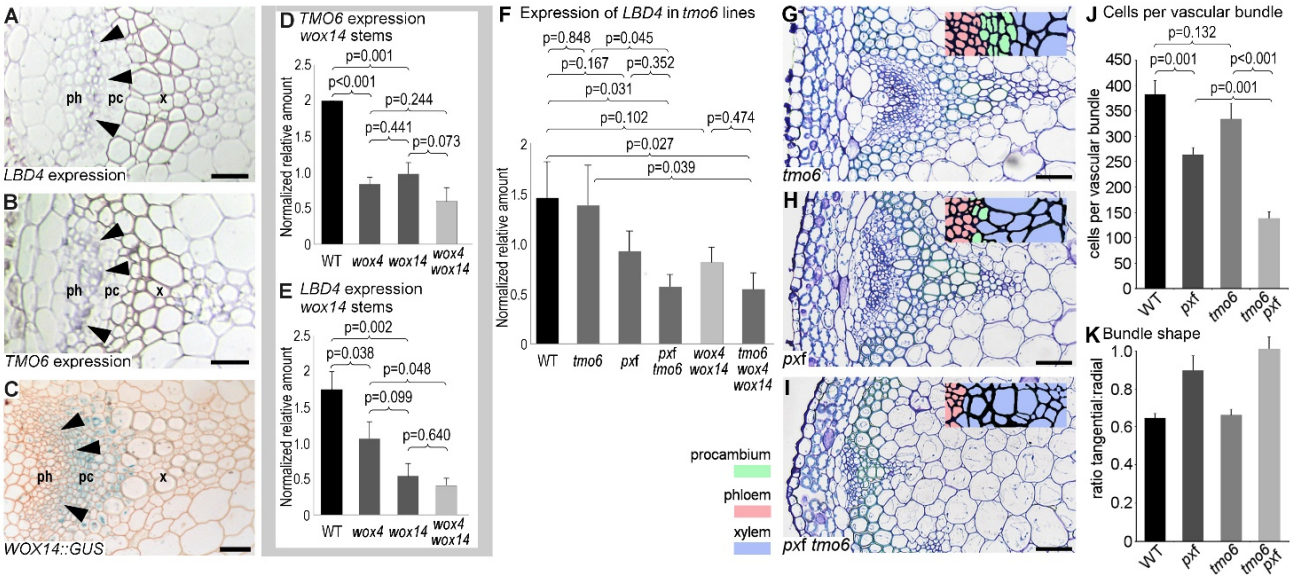

Figure 3. Gene expression studies supporting a regulatory relationship between *WOX14*, *TMO6* and *LBD4*

(**A-C**) *WOX14*, *TMO6* and *LBD4* demonstrate overlapping expression in inflorescence stem vascular bundles. Antisense probes against *LBD4* mRNA (A) or *TMO6* mRNA (B) localise to the phloem-procambium boundary. (C) *WOX14:GUS* transcriptional fusion showing the presence of broad *WOX14* expression in vascular bundles including at the phloem-procambium boundary (x marks xylem, pc marks cambium, ph marks phloem). (**D-E**) qRT-PCR on inflorescence stem tissue from the lower third of the stem showing that *TMO6* (D) and *LBD4* (E) expression is dependent on *WOX14*. (**F**) qRT-PCR showing that *TMO6* and *PXf* are required to maintain *LBD4* expression in the lower half of 15 cm inflorescence stems. Expression differences were determined in technical triplicate for each of three biological replicates. Tissue for each biological replicate was taken from a different pot. Statistical differences were determined with ANOVA and an LSD post-hoc test (n=3 biological replicates; error bars are standard error). (**G-I**) Vascular bundles from the inflorescence stems of *tmo6* (G), *pxy pxl1 pxl2* (*pxf*; H), and *pxf tmo6* (I) plants. Transverse sections were stained with toluidine blue. Scale bars are 30 µm. (**J**) Graph showing mean number of cells per vascular bundle. p values were determined with ANOVA and an LSD post-hoc test. (**K**) Histogram showing vascular bundle shape determined by measuring the ratio of tangential to radial axis. (n=6; error bars show standard error).

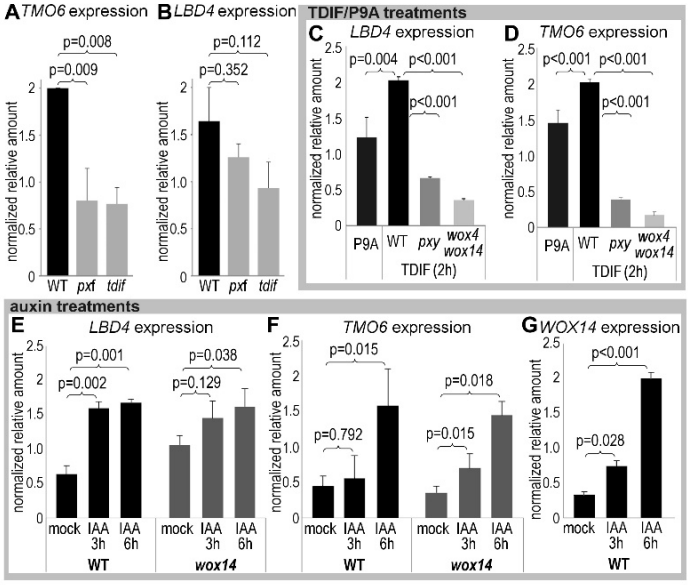

Figure 4. PXY and auxin signalling regulate the feed-forward loop
(**A-B**) qRT-PCR showing *TMO6* (A) and *LBD4* (B) expression in *pxf* and *tdif* lines. (**C-D**) *LBD4* (C) or *TMO6* (D) expression in seedlings treated with TDIF or P9A for 2 hours. (**E-G**) qRT-PCR showing *LBD4* (E), *TMO6* (F), and *WOX14* (G) expression in seedlings treated with IAA for 3 or 6 hours. Expression differences were determined in technical triplicate for each of three biological replicates. Tissue for each biological replicate was taken from a different plate. *p* values marked on critical comparisons were determined using ANOVA and an LSD post-hoc test (n=3 biological replicates; error bars are standard error). Bars show standard error; ANOVA with an LSD post-hoc test (n=3 pools).

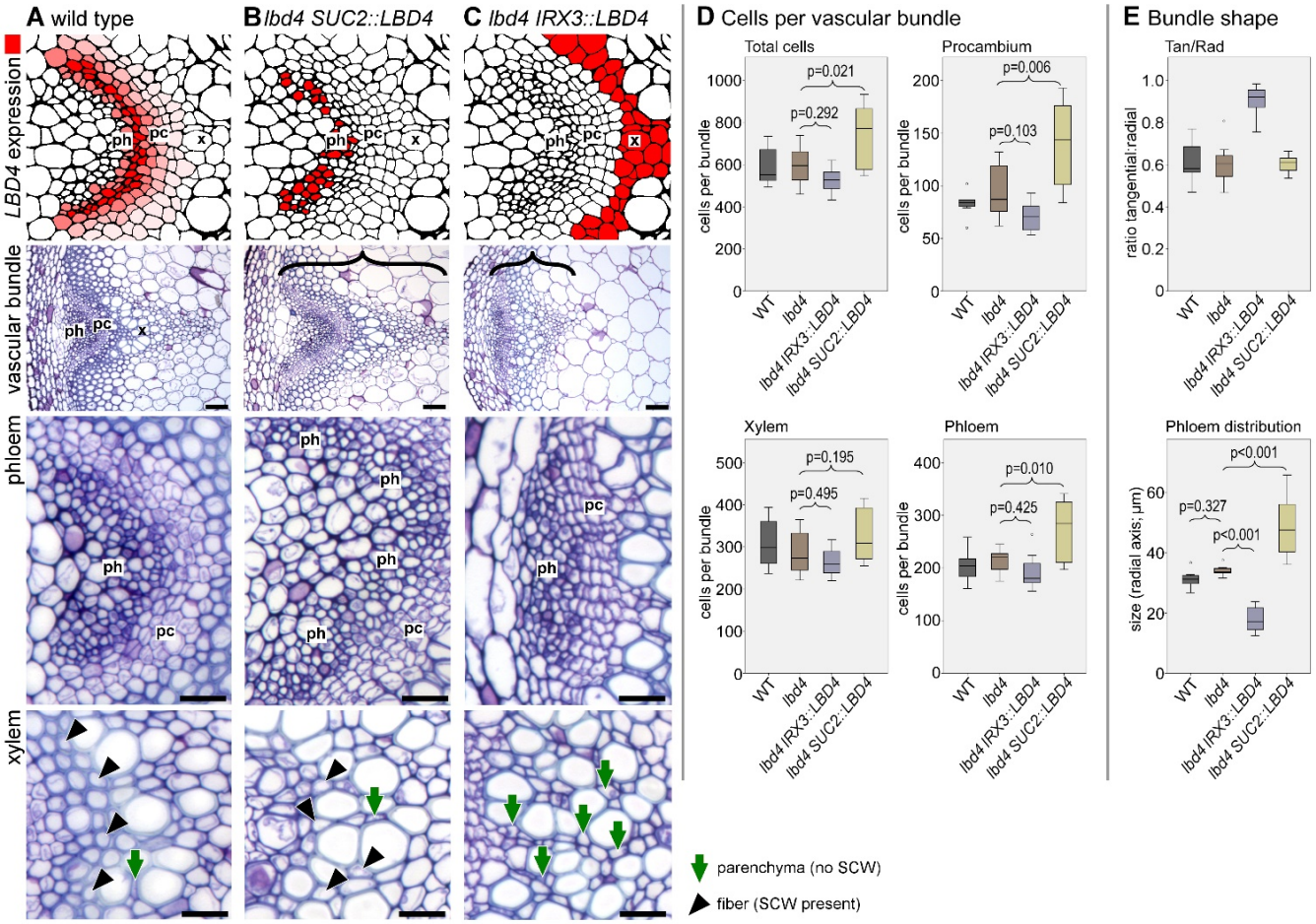

Figure 5. *LBD4* expression patterns the vascular tissue.

(**A-C**) Consequences of *LBD4* expression at the phloem-procambium boundary (A), in phloem (B), or in xylem (C) in inflorescence stems. Upper panels show diagrammatic representation of the *LBD4* expression domain with subsequent panels showing overall vascular morphology, phloem, and xylem. (A) Wild-type vascular bundle showing an arc of phloem cells, procambium cells and xylem cells along the radial axis of a stem transverse section. Xylem is characterised by the presence of fiber cells with large secondary cell walls (black arrowheads). (B) *lbd4 SUC2:LBD4* lines have an increase phloem size. Xylem fibre cells retain secondary cell walls (black arrowheads). Parenchyma, with no secondary cell wall is marked with a green arrow. (C) *lbd4 IRX3:LBD4* lines demonstrate a change to phloem morphology, as the characteristic arc is absent. Cells where fibres were observed in wild type xylem do not have large secondary cell walls (parenchyma; green arrows). ph is phloem, pc procambium, x is xylem, SCW is secondary cell wall. Scale bars are 50 µM (whole vascular bundle) or 20 µM (xylem and phloem close-ups). The radial axis is marked in (B) and (C) with a black bracket. (**D**) Boxplots showing the mean number of total cells per vascular bundle (upper left), number of procambium (upper right), phloem (lower right), and xylem (lower left) cells per vascular bundle. *p* values were determined using ANOVA with an LSD post-hoc test (n=7). (**E**) Upper boxplot shows vascular bundle shape determined by measuring the ratio of the tangential to radial axis, lower boxplot showing distribution of phloem along the radial axis of the stem. *p* values were determined using ANOVA with an LSD post-hoc test (n=7). Boxplots show median (inner line) and inner quartiles (IQ, box). Whiskers extend to the highest and lowest values no greater than 1.5 times the IQ range, circles show outliers.

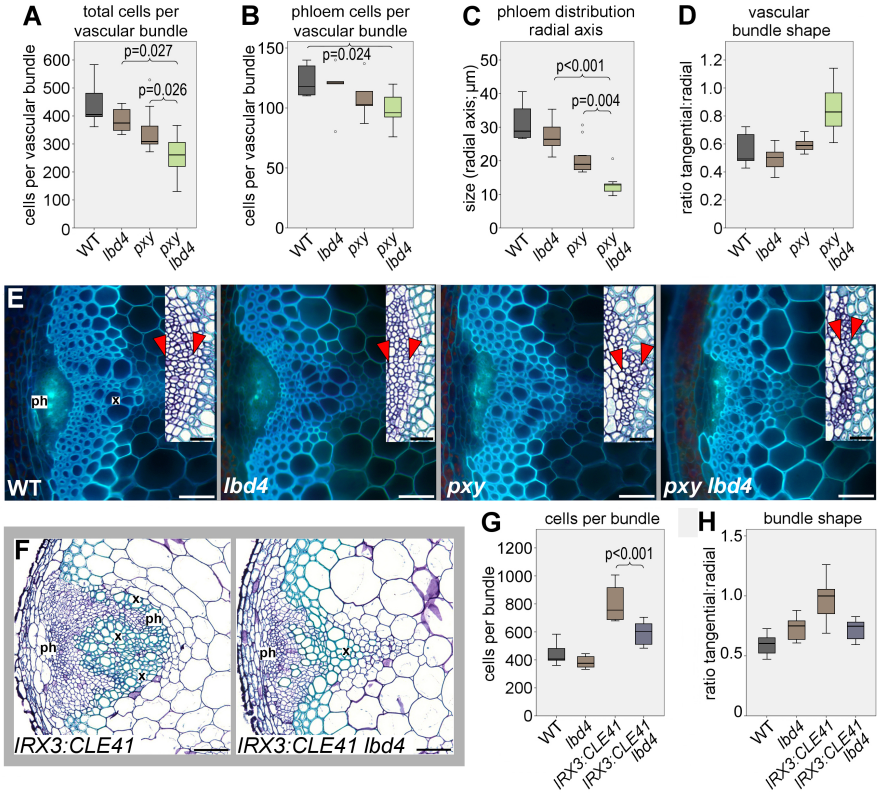

Figure 6. Genetic interactions between *LBD4* and *TDIF-PXY*.
(**A-E**) Analysis of *pxy lbd4* double mutants and controls. Boxplots showing the total number of cells (A; n=7), number of phloem cells (B; n=6)) per vascular bundle in 8-week-old inflorescence stems. (C) Boxplot showing distribution of phloem along the radial axis of the stem (distribution is shown on insets in (E) as tissue between the red arrowheads; n=7). (D) Boxplot showing vascular bundle shape determined by measuring the ratio of the tangential to radial axis (n=8). (E) Aniline blue stained transverse sections of wild type, *lbd4*, *pxy*, *pxy lbd4*. Insets show close up of phloem tissue stained with toluidine blue. (**F-H**) *lbd4* suppresses *CLE41* misexpression phenotypes. (F) *IRX3:CLE41* vascular bundles are characterised by organisation defects but these defects are attenuated in *IRX3:CLE41 lbd4* lines. Boxplots showing number of cells per vascular bundle, and vascular bundle shape determined by measuring the ratio of tangential to radial axis (n=6). 8-week-old plants were used. Scale bars are 50 µm, except for insets in (D) where scale bars are 20 µm. Bars show standard error; p values in (A-D) and (G) were determined using ANOVA with an LSD post-hoc test. ph is phloem, pc procambium, x is xylem. Boxplots show median (inner line) and inner quartiles (IQ, box). Whiskers extend to the highest and lowest values no greater than 1.5 times the IQ range, circles show outliers.